Cell Communication and Signaling

RESEARCH

Open Access

T-type voltage-gated channels, Na^+/Ca^{2+}-exchanger, and calpain-2 promote photoreceptor cell death in inherited retinal degeneration

Jie Yan[1,2,3†], Lan Wang[2,3†], Qian-Lu Yang[4], Qian-Xi Yang[4], Xinyi He[3,5], Yujie Dong[1], Zhulin Hu[1], Mathias W. Seeliger[6], Kangwei Jiao[1] and François Paquet-Durand[2*]

Abstract

Inherited retinal degenerations (IRDs) are a group of untreatable and commonly blinding diseases characterized by progressive photoreceptor loss. IRD pathology has been linked to an excessive activation of cyclic nucleotide-gated channels (CNGC) leading to Na^+- and Ca^{2+}-influx, subsequent activation of voltage-gated Ca^{2+}-channels (VGCC), and further Ca^{2+} influx. However, a connection between excessive Ca^{2+} influx and photoreceptor loss has yet to be proven.

Here, we used whole-retina and single-cell RNA-sequencing to compare gene expression between the *rd1* mouse model for IRD and wild-type (*wt*) mice. Differentially expressed genes indicated links to several Ca^{2+}-signalling related pathways. To explore these, *rd1* and *wt* organotypic retinal explant cultures were treated with the intracellular Ca^{2+}-chelator BAPTA-AM or inhibitors of different Ca^{2+}-permeable channels, including CNGC, L-type VGCC, T-type VGCC, Ca^{2+}-release-activated channel (CRAC), and Na^+/Ca^{2+} exchanger (NCX). Moreover, we employed the novel compound NA-184 to selectively inhibit the Ca^{2+}-dependent protease calpain-2. Effects on the retinal activity of poly(ADP-ribose) polymerase (PARP), sirtuin-type histone-deacetylase, calpains, as well as on activation of calpain-1, and − 2 were monitored, cell death was assessed *via* the TUNEL assay.

While *rd1* photoreceptor cell death was reduced by BAPTA-AM, Ca^{2+}-channel blockers had divergent effects: While inhibition of T-type VGCC and NCX promoted survival, blocking CNGCs and CRACs did not. The treatment-related activity patterns of calpains and PARPs corresponded to the extent of cell death. Remarkably, sirtuin activity and calpain-1 activation were linked to photoreceptor protection, while calpain-2 activity was related to degeneration. In support of this finding, the calpain-2 inhibitor NA-184 protected *rd1* photoreceptors.

These results suggest that Ca^{2+} overload in *rd1* photoreceptors may be triggered by T-type VGCCs and NCX. High Ca^{2+}-levels likely suppress protective activity of calpain-1 and promote retinal degeneration via activation of calpain-2. Overall, our study details the complexity of Ca^{2+}-signalling in photoreceptors and emphasizes the importance of targeting degenerative processes specifically to achieve a therapeutic benefit for IRDs.

† Jie Yan and Lan Wang shared first authors who contributed equally to this work.

*Correspondence:
François Paquet-Durand
francois.paquet-durand@klinikum.uni-tuebingen.de
Full list of author information is available at the end of the article

Keywords Retinitis pigmentosa, Calcium channels, cGMP, HDAC, PAR, SOCE

Introduction

Inherited retinal degenerations (IRDs) are a large group of genetically heterogeneous, potentially blinding diseases of the retina [1]. The most common form of IRD is *retinitis pigmentosa* (RP), with a prevalence of approximately 1:4000, affecting more than two million patients worldwide [2]. RP patients commonly experience reduced night vision due to primary degeneration of rod photoreceptors, and subsequently suffer from a progressive visual field constriction known as 'tunnel vision' due to a secondary degeneration of cone photoreceptors linked to the preceding rod loss [2]. The second messenger cyclic-guanosine-monophosphate (cGMP) has been identified to play a central role in the pathobiology of many genetically distinct types of IRD [3], and may be directly or indirectly associated with the activity of histone deacetylases (HDACs), poly(ADP-ribose) polymerases (PARPs), cyclic nucleotide-gated channels (CNGCs), and calpain-type proteases [3–5].

cGMP- and Ca^{2+}-signalling play a crucial role for the phototransduction, the first step of vision, in photoreceptors. cGMP is produced by guanylyl cyclase, the activity of which is inhibited by Ca^{2+} [5]. In darkness, cGMP opens CNGC, causing influx of Na^+ and Ca^{2+}. Together, Ca^{2+} and cGMP form a feedback loop which controls the levels of both second messengers. CNGC-mediated ion influx is countered by the $Na^+/Ca^{2+}/K^+$ exchanger (NCKX) and by the ATP-driven Na^+/K^+ exchanger (NKX) [5]. As a result, in the dark, a photoreceptor cell is depolarised at approximately −40 mV [6, 7]. The consequent activation of voltage-gated Ca^{2+}-channels (VGCCs) mediates further Ca^{2+} influx and synaptic glutamate release [6, 8]. In light, the enzyme phosphodiesterase-6 (PDE6) rapidly hydrolyses cGMP, leading to CNGC closure, Ca^{2+} decrease, and photoreceptor hyperpolarization. Subsequently, VGCCs close, ending synaptic neurotransmitter release [5]. In IRDs, a mutation-induced cGMP accumulation is likely to over-activate CNGCs and to produce an abnormal influx of Na^+ and Ca^{2+} into photoreceptors [9].

The *rd1* mouse is a naturally occurring IRD model first described by Keeler in the 1920s [10] and has been employed extensively as an animal model of retinitis pigmentosa [11]. It is characterized by early onset, rapid retinal degeneration due to a mutation in the rod-photoreceptor-specific *Pde6b* gene [12]. This causes dysfunction of cGMP-phosphodiesterase-6 (PDE6) and subsequent accumulation of cGMP in rods. This in turn results in primary rod degeneration, starting at postnatal day 9 (P9), with a peak of cell death at about P13, and with essentially all rods lost by P21. This is followed by secondary cone photoreceptor cell loss occurring between P18 to P60 [13, 14]. The primary *rd1* degeneration has often been connected to an excessive Ca^{2+} influx, notably through cGMP-dependent CNGCs [15]. Excessive Ca^{2+} is thought to promote activity of Ca^{2+}-dependent calpain-type proteases and *rd1* photoreceptor death [16]. Accordingly, many studies over the past decades have focused on the role of Ca^{2+} in IRDs, albeit without conclusive results until today [17]. While some studies indicated that Ca^{2+}-channel blockers or genetic ablation of Ca^{2+}-permeable channels may preserve photoreceptors [18, 19], other work suggested that inhibition of Ca^{2+}-permeable channels either does not reduce retinal cell death or may even promote degeneration [20, 21]. Overall, these conflicting results raise the question whether *rd1* rod cell death is linked to Ca^{2+} overload, and, if so, which Ca^{2+}-permeable channels might be responsible.

A candidate for a Ca^{2+}-permeable channel causing *rd1* pathology is VGCC. Functional VGCCs are composed of pore-forming α_1 subunit proteins, encoded by *CACNA1x* genes, of which there are 10 isoforms in the mammalian genome [22]. In the case of $Ca_V1.1$–1.4 channels (known as L-type channels), these are encoded by *CACNA1S*, *-C*, *-D* and *-F*, respectively. The $Ca_V2.1$–2.3 channels (termed P/Q-, N- and R-type) are encoded by *CACNA1A*, *-B* and *-E*, accordingly. The T-type $Ca_V3.1$–3.3 channels are encoded by *CACNA1G*, *-H* and *-I* [22, 23]. The accessory $\alpha_2\delta$ and β subunits are important for channel folding, subsequent transport to the cell surface, and their integration into specific domains in polarized cells such as neurons. Both Ca_V1 and Ca_V2 classes of channels form a heteromeric complex, co-assembling with one of four β subunits (encoded by *CACNB1-4*), and one of four $\alpha_2\delta$ subunits (encoded by *CACNA2D1-4*) [22].

Changes in membrane potential triggered by either CNGC or VGCC activity may affect the activity of the Na^+/Ca^{2+} exchanger (NCX). This is a bi-directional regulator of cytosolic Ca^{2+}, which in forward mode transports Ca^{2+} out of cells; however, in reverse mode NCX may import extracellular Ca^{2+} [24]. As NCX does not require ATP for ion transport, the direction of Ca^{2+} movement through the channel depends on the net electrochemical gradients for Na^+ and Ca^{2+}, such that membrane depolarization can augment Ca^{2+} influx [24]. Ion transport by the NCX is electrogenic, with a

stoichiometry of three Na^+ ions exchanged for each Ca^{2+} ion [25]. In mammals, three different NCX genes have been identified: *SLC8A1* encoding NCX1, *SLC8A2* encoding NCX2, and *SLC8A3* encoding NCX3 [26].

Store-operated Ca^{2+} entry (SOCE) is a ubiquitous Ca^{2+} signalling pathway, which is triggered physiologically when the endoplasmic reticulum (ER) Ca^{2+} stores are depleted. In this situation Ca^{2+}-levels are replenished through Ca^{2+}-release-activated Ca^{2+}-channels (CRAC) [27]. SOCE involves a complex choreography between the plasma membrane (PM) protein "Orai" (encoded by *ORAI1* and *ORAI2*) and the ER-resident Ca^{2+}-sensing stromal interaction molecules (STIMs, encoded by *STIM1* and *STIM2*). The depletion of ER Ca^{2+} is sensed by STIM1 and its homolog STIM2, causing the opening of Orai channels to drive Ca^{2+} entry into the cell [27].

Excessive Ca^{2+} may activate Ca^{2+}-dependent calpain-type proteases [16]. In the calpain family the isoforms calpain-1, calpain-2, and calpain-5 have been connected to neurodegenerative diseases [28–30]. The best-characterized calpain isoforms are calpain-1 and calpain-2 [30, 31], where the former is often linked to processes like synaptic plasticity and long-term potentiation, important for learning and memory [32]. Calpain-2 may have a more prominent role in cytoskeletal remodelling and cell motility [33]. Recent studies have suggested that calpain-1 and calpain-2 may play opposing roles, where calpain-1 may be neuroprotective while calpain-2 may be causing neurodegeneration [34].

To try and settle the long-standing controversy on the role of Ca^{2+} in IRD pathogenesis, we performed an initial bio-informatic analysis of differentially expressed genes (DEGs) in *rd1* mouse retina based on both whole-retina RNA sequencing (RNA-seq) and single-cell RNA sequencing (scRNA-seq) datasets. We found numerous DEGs to be enriched in Ca^{2+} associated pathways, arguing for an important function of Ca^{2+}-signalling. We then used Ca^{2+} chelation and Ca^{2+}-permeable channel inhibition in organotypic *rd1* retinal explant cultures to identify the possible sources of high photoreceptor Ca^{2+}. To assess the role of Ca^{2+}-dependent proteolysis, we also studied the overall activity of calpains, and then focussed on calpain-1 and −2. We found that calpain-2 contributed to photoreceptor cell death, a finding confirmed by the protective effect of the selective calpain-2 inhibitor NA-184. Altogether, we show that Ca^{2+} contributes to *rd1* photoreceptor cell death, regulating, among other things, the activity of PARPs and sirtuins, and that Ca^{2+} overload and photoreceptor degeneration is likely caused by T-type VGCC and NCX. Surprisingly, inhibition of either CNGC or CRAC did accelerate retinal degeneration.

Materials and methods

Animals

For retinal explant cultures C3H/HeA *Pde6b*$^{rd1/rd1}$animals (*rd1*), their congenic wild-type C3H/HeA *Pde6b*$^{+/+}$ counterparts (*wt*) [35], and B6.129SvJ;C3H/HeA-*CNGB1*^{tm} double-mutant mice (*rd1*Cngb1*$^{-/-}$) were used [19]. The *rd1*Cngb1*$^{-/-}$ double mutants were generated by an intercross of *rd1* and *Cngb1*$^{-/-}$ [19]. Animals were used regardless of gender. The stock has been maintained by repeated backcrossing over ten generations to make a congenic inbred strain, homozygous for both gene mutations.

In *rd1* mouse retina, rod photoreceptors start to degenerate at post-natal day (P) 9 with the peak of cell death occurring at P13 and the rod degeneration essentially complete by P21 [36]. The last time-point at which the overall retinal morphology and cellular composition of the retina is still comparable between *rd1* and wt retina is at P11. In *rd1*Cngb1*$^{-/-}$ double mutants, the degeneration progresses significantly slower, with the onset of rod death at around P12, the peak of cell death at P18 and the end of photoreceptor degeneration at around two months post-natal [19].

Animals were housed under standard white cyclic lighting and had free access to food and water. Animal protocols compliant with § 4 of the German law of animal protection were reviewed and approved by the competent authority (Einrichtung für Tierschutz, Tierärztlicher Dienst und Labortierkunde, Registration No. AK02/19M, AK01/20M AK05/22M).

Analysis of RNA-Seq, scRNA-seq data and differential expression

The mRNA expression comparison between *rd1* and *wt* mouse employed datasets downloaded from the GSE62020 database [37], while single-cell RNA expression analysis used data from the GSE212183 database [38]. To characterize *rd1*, we performed a differential analysis (fold change > 1.2, $p < 0.05$) [39, 40] comparing *rd1* to *wt* using the "limma" package of R language. Heatmaps and volcano plots used to visualize Ca^{2+}-related genes were created using the packages "pheatmap" and "ggplot2". To infer functional annotations of *rd1* genes, gene ontology (GO) [m5.go.v2022.1.Mm.symbols.gmt] of differentially expressed genes (DEGs) was supplemented by gene set enrichment analysis (GSEA; version 4.2.2). The statistical significance was defined as false discovery rate (FDR) < 0.05, and the overrepresentation of indicated GO gene sets in the ranked gene lists were presented by the normalized enrichment score (NES). GO enrichment analyses were conducted for the selected common DEGs using "GOplot" and "enrichplot" packages, $p < 0.05$. Additionally, the software packages "ggpubr", "corrplot",

"fmsb" and "ggalluvial" were used to generate box plot, balloon plot, deviation plot, correlation plot, radar plot, and alluvial diagram, respectively.

Retinal explant culture

To study the effects of various drugs on photoreceptor enzyme activities and cell death, we used organotypic retinal explant cultures derived from *wt*, *rd1*, and *rd1*Cngb1*$^{-/-}$ animals. Mouse retinal explants can be maintained under defined conditions for culturing periods of at least four weeks, with only minor cell loss induced by the culture situation [41, 42]. Retinas were explanted at postnatal day 5 (P5). The explants were cultured on a polycarbonate membrane (Order No.: 83.3930.040; 0.4 µm TC-inserts, SARSTEDT, Hildesheim, Germany) with complete medium (Gibco R16 medium with supplements) [43]. The two retinas obtained from a single animal were split across different experimental groups to maximize the number of independent observations acquired per animal. After explantation, the complete R16 medium was changed every two days along with the pharmaceutical compounds including 10 µM BAPTA-AM [44] (ab120503; Abcam, Cambridge, UK), 50µM L-cis-diltiazem [45] (ab120532; Abcam), 20 µM CM4620 [46] (HY-101942; MedChemExpress, Sollentuna, Sweden), 40 µM SN-6 [47] (HY-107658; MedChemExpress), 100 µM D-cis-diltiazem [45] (ab120260; Abcam), 10 µM TTA-A2 [48] (HY-111828; MedChemExpress), 15 µM DS5565 [49] (HY-108006; MedChemExpress), and 1 µM NA-184 [50] (kindly provided by Michel Baudry, Western University, Pomona, CA, USA), respectively. The dosing of compounds was chosen based on the published IC_{50} values (see references given behind each compound) and the retinal dose-responses curves collected in Figure S2. All compounds were dissolved in DMSO at a final medium concentration of no more than 0.1% DMSO. Cultures were ended at P11 (*rd1* short-term cultures), P23 (*rd1* long-term treatment) and P17 (*rd1*Cngb1*$^{-/-}$) by either fixation with 4% paraformaldehyde (PFA) or without fixation and direct freezing in liquid N_2. Explants were embedded in Tissue-Tek (Sakura Finetek Europe B.V., Alphen aan den Rijn, The Netherlands) and sectioned (14 µm) in a cryostat (Thermo Fisher Scientific, CryoStar NX50 OVP, Runcorn, UK).

TUNEL staining

TUNEL (terminal deoxynucleotidyl transferase dUTP nick end labelling) assay kit (Roche Diagnostics, Mannheim, Germany) was used to label dying cells. Histological sections from retinal explants were dried and stored at − 20 °C. The sections were rehydrated with phosphate-buffered saline (PBS; 0.1 M) and incubated with proteinase K (1.5 µg/µL) diluted in 50 mM TRIS-buffered saline (TBS; 1 µL enzyme in 1 mL TBS) for 15 min. This was followed by 3 times 5 min TBS washing and incubation with blocking solution (10% normal goat serum, 1% bovine serum albumin, and 1% fish gelatine in phosphate-buffered saline with 0.03% Tween-20). TUNEL staining solution was prepared using 21 parts of blocking solution, 18 parts of TUNEL labelling solution, and 1 part of TUNEL enzyme. After blocking, the sections were incubated with TUNEL staining solution overnight at 4 °C. Finally, sections were washed 2 times with PBS, mounted using mounting medium with DAPI (ab104139; Abcam), and imaged by microscopy.

Calpain activity assay

This assay allows resolving the overall calpain activity in situ on unfixed tissue sections. Retinal tissue sections were incubated and rehydrated for 15 min in a calpain reaction buffer (CRB) (25 mM HEPES, 65 mM KCl, 2 mM $MgCl_2$, and 1.5 mM $CaCl_2$ in ddH_2O; pH 7.2) with 2 mM dithiothreitol (DTT). Tissue sections were incubated for 3 h at 37 °C in CRB with tBOC-Leu-Met-CMAC (25 µM; A6520; Thermo Fisher Scientific, OR, USA). Then, sections were washed with PBS and incubated with ToPro (1:1000 in PBS, Thermo Fisher Scientific) for 15 min. Afterwards, tissue sections were washed twice in PBS (5 min) and mounted using Vectashield without DAPI (Vector Laboratories Inc., Burlingame, CA, USA) for immediate visualization by microscopy.

PARP activity and PAR staining

The PARP in situ activity assay is based on the incorporation of a fluorescent NAD^+ analogue and allows resolving the overall PARP enzyme activity on unfixed tissue sections [51]. Such sections were incubated and rehydrated for 10 min in PBS. The reaction mixture (10 mM $MgCl_2$, 1mM dithiothreitol, and 50 µM 6-Fluo-10-NAD^+ (Cat. Nr.: N 023; Biolog, Bremen Germany) in 100 mM Tris buffer with 0.2% Triton X100, pH 8.0) was applied to the sections for 3 h at 37 °C. After three 5 min washes in PBS, sections were mounted in Vectashield with DAPI (Vector Laboratories) for subsequent microscopy.

For the detection of PAR, we used an immunostaining enhanced with 3,3′-diaminobenzidine (DAB) staining. The procedure is initiated by quenching of endogenous peroxidase activity using 40% MeOH and 10% H_2O_2 in PBS with 0.3% Triton X-100 (PBST) in retinal tissue sections for 20 min. Sections were further incubated with 10% normal goat serum (NGS) in PBST for 30 min, followed by anti-PAR antibody (1:200; ALX-804-220-R100; Enzo Life Sciences, Farmingdale, NY, USA) incubation overnight at 4 °C. Incubation with the biotinylated secondary antibody (1:150, Vector in 5% NGS in PBST) for 1 h was followed by the Vector ABC Kit (Vector

Laboratories, solution A and solution B in PBS, 1:150 each) for 1 h. DAB staining solution (0.05 mg/mL NH_4Cl, 200 mg/mL glucose, 0.8 mg/mL nickel ammonium sulphate, 1 mg/mL DAB, and 0.1 vol. % glucose oxidase in phosphate buffer) was applied evenly, incubated for precisely 3 min, and immediately rinsed with phosphate buffer to stop the reaction. Sections were mounted in Aquatex (Merck, Darmstadt, Germany).

Sirtuin/HDAC activity assay

This assay allows detecting overall HDAC activity in situ on fixed tissue sections and is based on an adaptation of the FLUOR DE LYS®-Green System (Biomol, Hamburg, Germany). Retinal sections were exposed to 50 µM FLUOR DE LYS®-SIRT1 deacetylase substrate (BML-KI177-0005; ENZO, New York, USA) with 2 mM NAD^+ (BML-KI282-0500; ENZO) in assay buffer (50 mM Tris/HCl, 137 mM NaCl; 2.7 mM KCl; 1mM MgCl2; pH 8.0) for 3 h at 37 °C. Sections were then washed in PBS and fixed in methanol at -20 °C for 20 min. Slides were mounted with FLUOR DE LYS® developer II concentrate (BML-KI176-1250; Enzo, New York, USA) diluted 1:5 in assay buffer overnight for subsequent microscopy.

Immunohistochemistry for calpain-1/2 and NCXs

Sections were rehydrated with PBS for 15 min and then incubated with a blocking solution (10% NGS, 1% BSA, and 0.3% PBST) for 1 h. The primary antibodies, rabbit-anti-calpain-2 (1:200; ab39165; Abcam), rabbit-anti-calpain-1 (1:100; ab39170; Abcam), rabbit-anti-NCX1 (1:200; LS-B15461; LifeSpan BioScience, Washington, USA), rabbit-anti-NCX2 (1:200; BS-1997R; BIOSS; Massachusetts, USA) and mouse-anti-NCX3 (1:100; NB120-2869; Novus Biologicals, Colorado, USA) were diluted in blocking solution and incubated overnight at 4 °C rinsing with PBS for 3 times 10 min each; this was followed by incubation with the secondary antibodies, goat-anti-rabbit AlexaFluor488 (1:400; A11034; Molecular Probes; Oregon, USA), goat-anti-rabbit AlexaFluor568 (1:300; A11036; Molecular Probes), and goat-anti-mouse AlexaFluor568 (1:500; A11031; Molecular Probes), for 1 h. The sections were further rinsed with PBS for 3 times 10 min each and mounted with mounting medium with DAPI (Abcam).

Microscopy and image analysis in retinal cultures

Images of organotypic explant cultures were captured using a Zeiss Imager Z.2 fluorescence microscope, equipped with ApoTome 2, an Axiocam 506 mono camera, and HXP-120V fluorescent lamp (Carl Zeiss Microscopy, Oberkochen, Germany). Excitation (λExc.)/emission (λEm.) characteristics of filter sets used for different fluorophores were as follows (in nm): DAPI (λExc. = 369 nm, λEm = 465 nm), AF488 (λExc. = 490 nm, λEm = 525 nm), AF568 (λExc. = 578 nm, λEm = 602 nm), and ToPro (λExc. = 642 nm, λEm = 661 nm). The Zen 2.3 blue edition software (Zeiss) captured images (tiled and z-stack, 20× magnification). Sections of 14 µm thickness were analysed using 15 Apotome Z-planes.

For quantification of positive cells in ONL, we proceeded as follows: The number of cells in six different rectangular ONL areas was counted manually based on the number of DAPI-stained nuclei and used to calculate an average ONL cell size. This average ONL cell size was used to calculate the total number of cells in a given ONL area. The percentage of positive cells was then calculated by dividing the absolute number of positive cells by the total number of ONL cells. ONL thickness was determined by manual counts on DAPI stained retinal sections. For each count, a vertical column was placed on nine different positions of the section and the end-to-end distances of the photoreceptor layer in each of these positions were recorded manually. The nine individual counts were averaged to give the mean value of photoreceptor thickness for one explant.

Statistical analysis and figure preparation

Two-way comparisons were analysed using Student's *t*-test. Multiple comparisons were made using a one-way analysis of variance (ANOVA) test with Tukey multiple comparison post-hoc test. Calculations were performed with GraphPad Prism 8 (GraphPad Software, La Jolla, CA, USA). Levels of significance were as follows: *, $p < 0.05$; **, $p < 0.01$; ***, $p < 0.001$; ****, $p < 0.0001$. Data in Fig. 8A was normalized by linear scaling according to the formula: $\chi_{scaled} = \chi\text{-}\chi_{min}/\chi_{max}\text{-}\chi_{min,}$ using SPSS Statistics 26 (IBM, Armonk, New York, USA). The figures were prepared using Photoshop 2022 and Illustrator 2022 (Adobe, San Jose, CA, USA). Bioinformatic analyses were performed by R software (Version 4.0.1). Figure 9 was created using BioRender.com.

Results

Ca^{2+}-related genes and pathways during the photoreceptor degeneration of *rd1*

To investigate whether and to what extent Ca^{2+} was involved in the progression of *rd1* retinal cell death, we initially performed RNA-seq to assess gene expression differences between *rd1* and *wt* mice at post-natal day (P) 13. The GSE62020 database [37] (accessed June 2023) was analysed to identify differentially expressed genes (DEGs). A fold change > 1.2 and a *p*-value < 0.05 were considered to indicate significant changes [39, 40]. Compared to *wt*, *rd1* retina expressed 666 up-regulated genes and – coincidentally – 667 down-regulated genes at P13 (Table S1). Among these, 89 DEGs

were found to be associated with Ca^{2+}-signalling, of which 32 were down-regulated and 57 were up-regulated in *rd1* retina (Fig. 1A). Gene set enrichment analysis (GSEA) revealed four gene ontology (GO) terms involved in Ca^{2+}-signalling (Fig. 1B, FDR < 0.05). Ten Ca^{2+}-related biology processes (BPs) and molecular

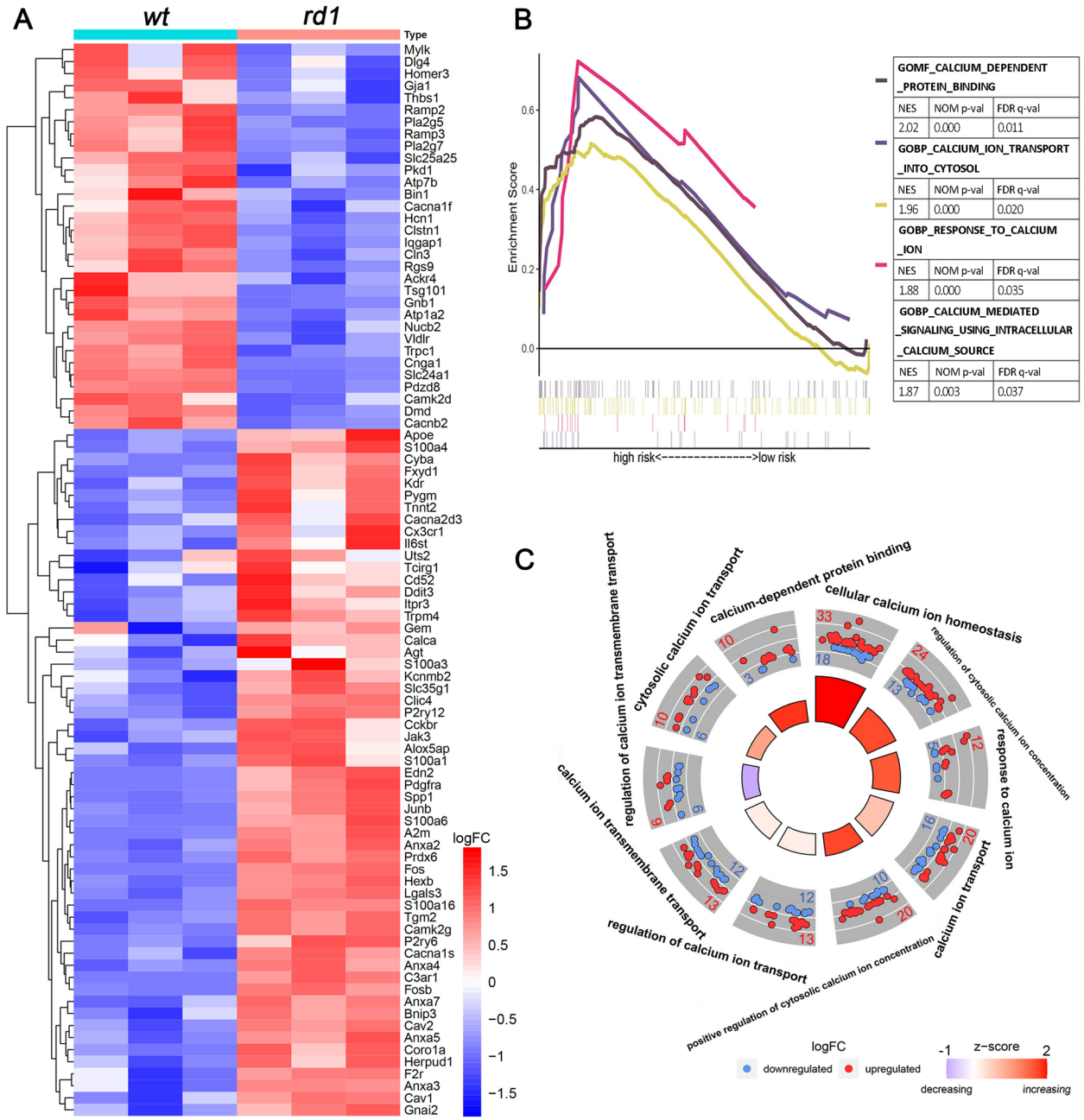

Fig. 1 Whole tissue RNA-seq analysis highlights Ca^{2+}-signalling-related changes in *rd1* retina. **A** Heatmap for post-natal day 13 RNA-Seq data comparing the expression of Ca^{2+}-related differentially expressed genes (DEGs) between *rd1* and wild-type (*wt*) retina. In this group of genes, 32 were down- and 57 were up-regulated in *rd1* retina. Color-coding indicates the logFC values (positive values in red, negative values in blue). **B** Gene set enrichment analysis (GSEA) showing upregulation of four Ca^{2+}-related gene ontology (GO) pathways in *rd1* retina (false discovery rate, FDR < 0.05). **C** Circle plot showing 10 different Ca^{2+}-related GO terms (including biological processes (BPs) and molecular functions (MFs)) enriched in DEGs in the *rd1* situation ($p < 0.05$). Color-coding of circles indicates the logFC values (positive values in red, negative values in blue); numbers in trapezoids indicate differentially expressed genes (red: upregulated; blue: downregulated); inner circle shows z-scores (increasing scores in red, decreasing scores in blue)

functions (MFs) were identified by DEGs GO enrichment analysis (Fig. 1C, $p < 0.05$).

Ca^{2+} plays an important role during photoreceptor degeneration

To further investigate Ca^{2+}-related pathways specifically in degenerating *rd1* photoreceptors, we performed single-cell (sc) RNA-seq analysis to assess transcriptional differences between the *rd1* and *wt* situation. A visualization in the form of a volcano plot showed the genes up- or down-regulated in rod photoreceptors from GSE212183 [38]. In total, 1233 DEGs were found to be differentially expressed between *rd1* and *wt* rod photoreceptors at P13, where 655 DEGs were up-regulated and 578 were down-regulated (Figure S1A, Table S2). 74 Ca^{2+}-related genes in rod photoreceptors are presented, of which 19 were down-regulated and 55 were up-regulated (Fig. 2A). These rod DEGs were linked to 19 Ca^{2+}-related GO terms (Table S4), among which the top-5 GO terms for rod photoreceptors were selected (Fig. 2B). There were 779 DEGs found in *rd1* cone photoreceptors at P13 (Figure S1B, Table S3). 38 Ca^{2+}-related genes were differentially expressed in cone photoreceptors, of which 11 were down-regulated and 27 were up-regulated (Fig. 2C). These cone DEGs were enriched in 6 Ca^{2+}-related biological processes (BP) (Table S5), the top-5 BP are shown (Fig. 2D).

In the following, we used the Ca^{2+} chelator BAPTA-AM in *rd1* organotypic retinal explants, with the aim of confirming the link between Ca^{2+} and photoreceptor degeneration. The TUNEL assay was used to quantify the numbers of dying cells in the outer nuclear layer (ONL). A dose-response for BAPTA-AM treatment on *rd1* explants was established and revealed 10 µM as a suitable concentration for further experiments (Figure S2A). In *wt* retinal explants, a relatively low number of ONL cells (1.08% ± 0.21, $n = 4$) were positive for the TUNEL assay, when compared with their *rd1* counterparts (4.84% ± 0.73, $n = 10$). BAPTA-AM treatment significantly reduced *rd1* ONL cell death to 3.34% (± 0.92, $n = 19$, $p < 0.001$; Fig. 2E). While BAPTA-AM treatment appeared to be well tolerated in *wt* retina (Figure S1D), it did not preserve photoreceptor viability in long-term treatment of *rd1* retina lasting until P23 (Figure S3A). In contrast, BAPTA-AM accelerated photoreceptor degeneration in explant cultures derived from *rd1*Cngb1*$^{-/-}$ double-mutant mice (Figure S1C), indicating that depletion of intracellular Ca^{2+} in photoreceptors lacking functional CNGC was detrimental.

Expression of Ca^{2+} permeable channels in retina and rod photoreceptors

A whole range of Ca^{2+}-permeable channels may potentially contribute to increased intracellular Ca^{2+}-levels in photoreceptors. Notably, the second messenger cGMP activates photoreceptor CNGC, leading to Na^+ and Ca^{2+} influx and, indirectly, via ensuing changes in membrane polarization, to additional Ca^{2+}-influx through VGCC [5]. High intracellular Na^+ levels produced by CNGC may reverse the directionality of NCX [52], possibly resulting in Ca^{2+}-influx instead of efflux. Moreover, high Ca^{2+}, via the activation of calmodulin-dependent protein kinase 2 (CaMK2), may potentiate Ca^{2+}-influx mediated by CRAC [53].

To assess the expression of these four groups of Ca^{2+}-permeable channels, we used RNA-seq and scRNA-seq to screen for any possible expression changes connected to *rd1* photoreceptor degeneration. While in whole retina RNA-seq numerous changes were found in genes encoding for CNGC, VGCC, CRAC, and NCX isoforms, the most prominent expression changes appeared after P18, i.e. at a time when most *rd1* rod photoreceptors have already been lost (Fig. 3A). At P13, RNA-seq data indicated that genes coding for VGCC were up-regulated while genes coding for CNGC were down-regulated (Fig. 3B). To pinpoint *rd1* photoreceptor specific gene expression changes in Ca^{2+}-permeable channels, we used scRNA-seq to investigate the critical P11 to P17 time-frame (Fig. 3C; cf. Figure S3B for a corresponding scRNA-seq analysis for cone photoreceptors). At the peak of photoreceptor degeneration, at P13, we found an upregulation of genes coding for CNGC, VGCC, and NCX (Fig. 3D), while CRAC genes appeared to be down-regulated. However, we also found an upregulation in

(See figure on next page.)

Fig. 2 Photoreceptor scRNA-Seq and Ca^{2+} chelation reveal critical role for Ca^{2+}-signalling in *rd1* cell death. **A** Volcano plot for scRNA-Seq data showing Ca^{2+}-related differentially expressed genes (DEGs) in *rd1 vs.* wild-type (*wt*) rod photoreceptors. **B** Circle plot showing top-5 Ca^{2+}-related GO terms enriched for Ca^{2+}-related DEGs in *rd1* rod photoreceptors ($p < 0.05$). **C** Volcano plot for scRNA-Seq data showing Ca^{2+}-related differentially expressed genes (DEGs) in *rd1 vs.* wild-type (*wt*) cone photoreceptors. **D** Circle plot showing top-5 Ca^{2+}-related GO terms enriched for Ca^{2+}-related DEGs in *rd1* cone photoreceptors ($p < 0.05$). **E** The TUNEL assay labelled dying cells (magenta) in *wt* and *rd1* retinal explant cultures. DAPI (grey) was used as nuclear counterstain. Untreated (Untr.) *wt* and *rd1* retina were compared to retina treated with 10 µM BAPTA-AM (BAPTA). Scatter plot displaying percentage of TUNEL-positive cells in the outer nuclear layer (ONL). Statistical testing: Student's *t*-test performed between *rd1* Untr. and 10 µM BAPTA-AM (BAPTA). Untr. *wt*: $n = 4$; Untr. *rd1*: 10; BAPTA *rd1*: 19; error bars represent SD; *** = $p < 0.001$. INL = inner nuclear layer, GCL = ganglion cell layer; scale bar = 50 µm

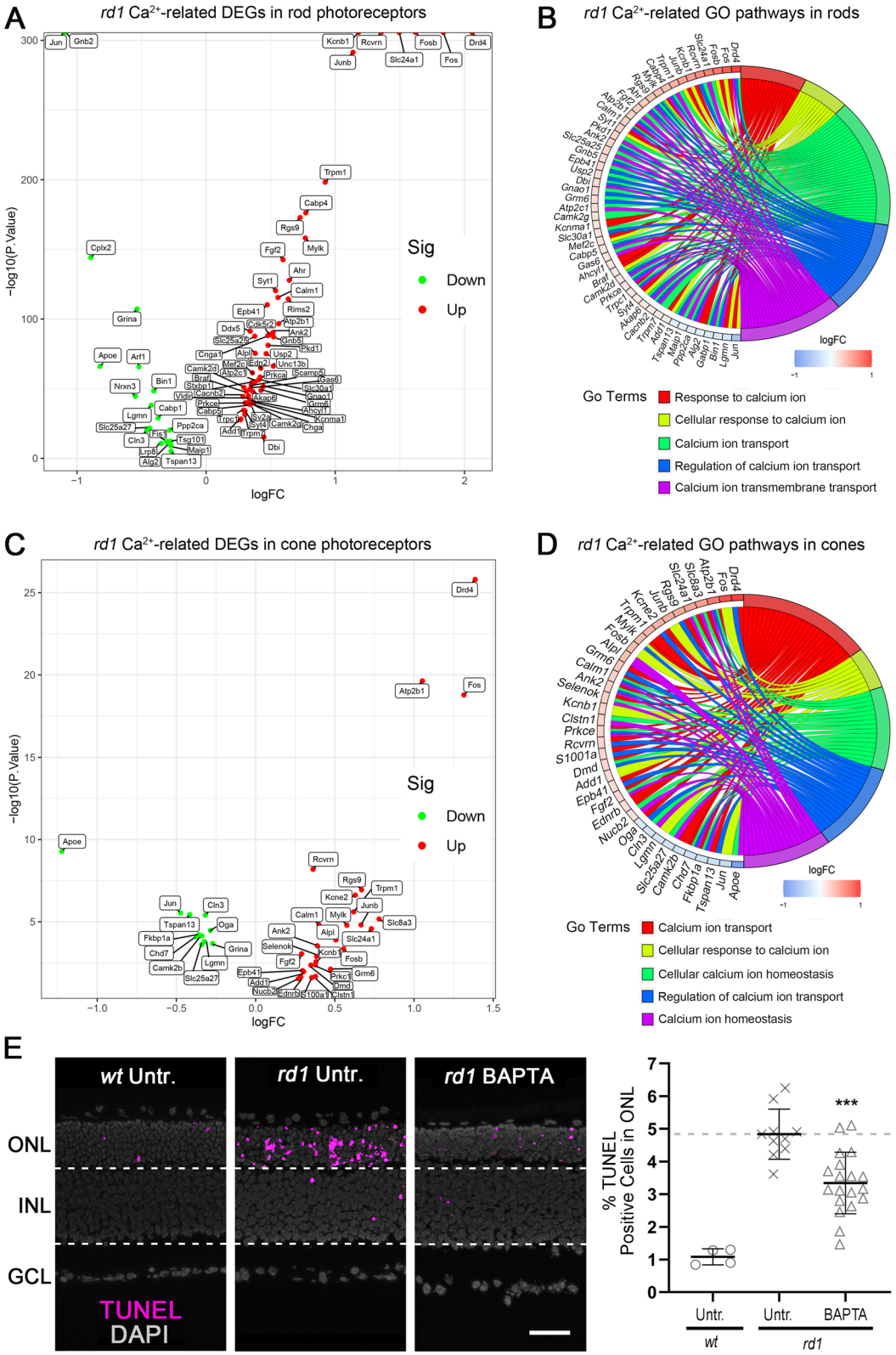

Fig. 2 (See legend on previous page.)

the expression of the *Camk2g* gene, where CaMK2 may increase CRAC activity independent of CRAC gene expression changes (Figure S3C).

Overall, the RNA-seq and scRNA-seq data suggested important changes in the expression of Ca^{2+}-permeable channel-related genes in *rd1* photoreceptor degeneration. Still, from the RNA expression data alone it was not possible to unambiguously deduce which type of Ca^{2+}-permeable channel was causally involved in *rd1* cell death.

Inhibition of Ca^{2+} permeable channels impact rod photoreceptor viability

To characterize the role of different Ca^{2+}-permeable channels functionally, we employed an array of different channel inhibitors, including the CNGC inhibitor L-cis-diltiazem (L-cis), the CRAC inhibitor CM4620, the NCX inhibitor SN-6, the L-type VGCC inhibitor D-cis-diltiazem (D-cis), the T-type VGCC inhibitor TTA-A2, and the $\alpha_2\delta$ subunit VGCC ligand DS5565. Retinal explant cultures derived from *rd1* and *wt* animals were treated with these inhibitors and the effects analysed using the TUNEL assay to detect dying cells in the ONL. To assess a possible cross-reactivity of the inhibitors used, we also employed explant cultures derived from *rd1*Cngb1*$^{-/-}$ double-mutant mice, i.e. retinas in which rods lack functional CNGC. For L-cis and D-cis suitable drug concentrations for retinal treatments had been established previously [45]; for inhibitors where such data were missing (i.e. SN-6, TTA-A2, DS5565, CM4620), dose-response curves were generated to select appropriate treatment concentrations (Figures S2).

As shown previously [16, 54], in *wt* retina the number of TUNEL positive cells in the ONL was significantly lower than in its *rd1* counterpart (Fig. 3E, Table S6). Remarkably, treatment with both L-cis and CM4620 significantly increased the numbers of TUNEL positive cells in both *rd1* and *wt* ONL (Fig. 3E, Figure S1D, Table S6). In other words, L-cis and CM4620 exhibited clear photoreceptor toxicity that was independent of the *rd1* mutation. In contrast, SN-6 and TTA-A2 significantly decreased photoreceptor cell death in *rd1* retina (Fig. 3E, Table S6). Also, in the retina of *rd1*Cngb1*$^{-/-}$ double-mutant mice SN-6 significantly decreased TUNEL positive cells (Figure S1C), yet, in *wt* retina ONL cell death was significantly increased by SN-6 (Figure S1D). Like BAPTA-AM, SN-6 did not show long-term protection in *rd1* ONL (Figure S3A). To assess the expression of NCX at the protein level, immunostaining was performed using antibodies directed against NCX1, NCX2, and NCX3. When compared to negative control, only NCX1 was found to be expressed in *rd1* and *wt* retina, notably in photoreceptor segments and Müller glial cells (Figure S3D).

The compounds D-cis and DS5565 targeting L-type and $\alpha_2\delta$ VGCC did not lead to significant reduction of TUNEL positive cells in *rd1* ONL (Fig. 3E, Table S6).

Taken together, the experiments with Ca^{2+}-permeable channel blockers confirmed that Ca^{2+}-signalling was indeed important for photoreceptor viability. Contrary to expectations, activity of CNGC and CRAC appeared to have a pro-survival role, while activity of T-type VGCC and NCX was detrimental for *rd1* rod photoreceptors. The role of NCX appeared ambiguous, as its inhibition improved survival of *rd1* photoreceptors but promoted death in *wt* ones, suggesting that NCX directionality might have been reversed in the *rd1* situation. Finally, L-type VGCC activity appeared to be unrelated to *rd1* degeneration.

Calpain-2 contributes to *rd1* photoreceptor degeneration

The reduction of TUNEL-positive cells after Ca^{2+} chelation and Ca^{2+} permeable channel inhibition strongly pointed to a link between high intracellular Ca^{2+}-levels and *rd1* photoreceptor cell death. To further investigate Ca^{2+}-induced cell death, we performed GSEA analysis

(See figure on next page.)

Fig. 3 Inhibition of differentially expressed Ca^{2+}-channels in *rd1* retina either promote or reduce photoreceptor cell death. **A** Balloon plot showing time-dependent whole-retina expression changes (post-natal day (P) 7 to P21) of cyclic nucleotide-gated channel (CNGC), Ca^{2+}-release activated channel (CRAC), Na^+/Ca^{2+} exchanger (NCX), and voltage-gated Ca^{2+} channel (VGCC). **B** Deviation plot highlighting expression changes for CNGC, CRAC, NCX, and VGCC in P13 *rd1* whole retina. **C** Balloon plot showing scRNA-seq data and time-dependent expression changes (post-natal day (P) 11 to P17) of CNGC, CRAC, NCX, and VGCC in *rd1* rod photoreceptors. **D** Deviation plot highlighting expression changes for CNGC, CRAC, NCX, and VGCC in P13 *rd1* rod photoreceptors. **E** TUNEL assay labelling dying cells (magenta) in *rd1* and wild-type (*wt*) retinal explant cultures. DAPI (grey) was used as a nuclear counterstain. Untreated (Untr.) *wt* and *rd1* retina were compared to retina treated with 50 µM CNGC inhibitor (L-cis diltiazem), 20 µM CRAC inhibitor (CM4620), 40 µM NCX inhibitor (SN-6), 100 µM L-type VGCC inhibitor (D-cis diltiazem), 10 µM T-type VGCC inhibitor (TTA-A2), and 15 µM $\alpha_2\delta$ subunit VGCC ligand (DS5565). Scatter plot showing percent TUNEL-positive cells in outer nuclear layer (ONL). Dashed line indicates *rd1* untr. situation, data points below this threshold indicate protective effects, data points above suggest destructive effects. Statistical testing: one-way ANOVA and Tukey's multiple comparison post hoc test. Untr. *wt*: $n = 5$; Untr. *rd1*: 18; L-cis *rd1*: 6; CM4620 *rd1*: 15; SN-6 *rd1*: 9; D-cis *rd1*: 12; TTA-A2 *rd1*: 6; DS5565 *rd1*: 6; error bars represent SD; significance levels: *** = $p < 0.001$; **** = $p < 0.0001$. INL = inner nuclear layer, GCL = ganglion cell layer; scale bar = 50 µm

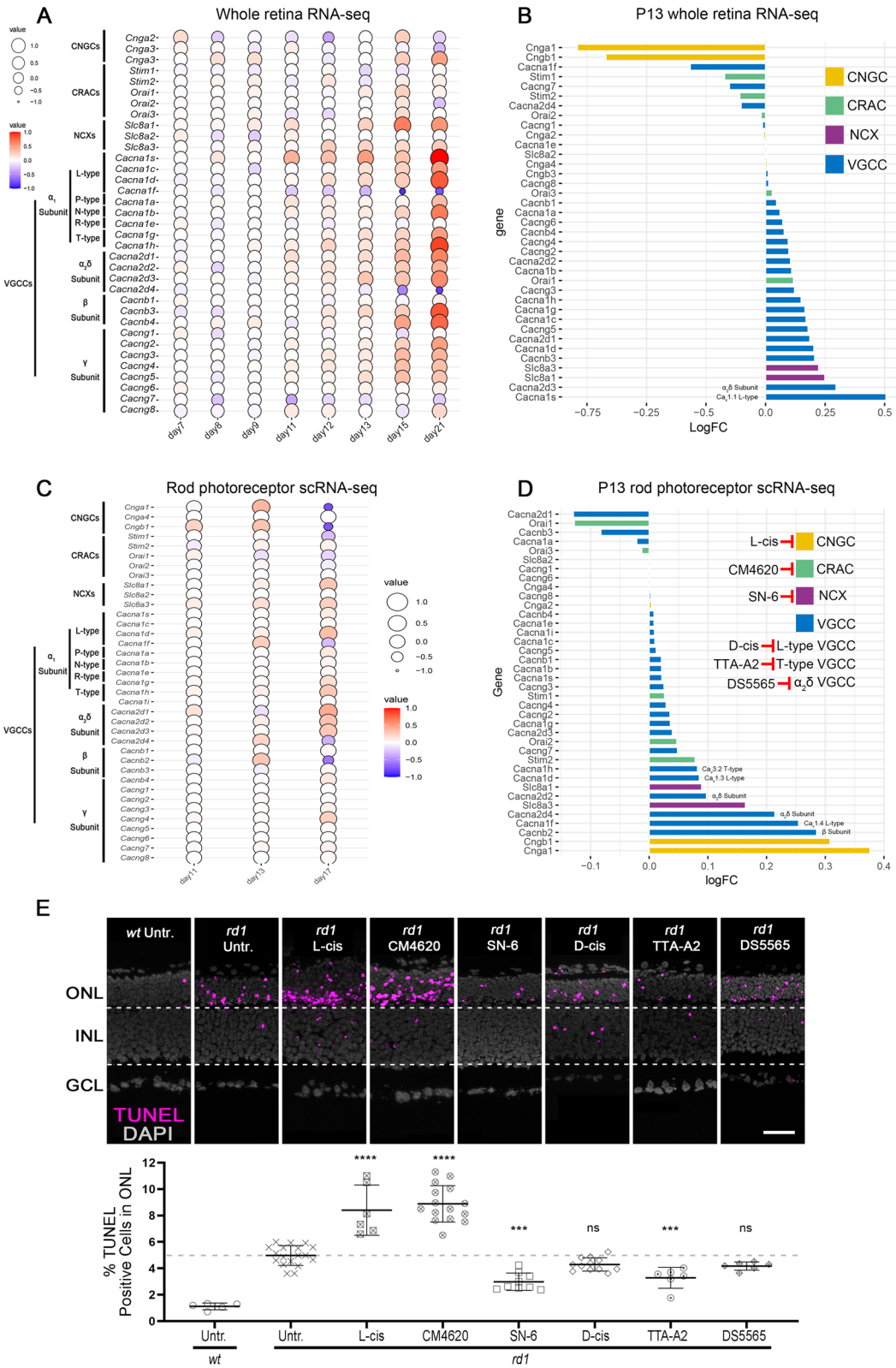

Fig. 3 (See legend on previous page.)

on *rd1* P13 RNA-seq data, in which DEGs were enriched in the GO biological process (BP) pathways, including "Positive regulation of proteolysis" (GO: 0045862; normalized enrichment score (NES) = 1.78, $p < 0.0001$; Fig. 4A), "Membrane protein proteolysis" (GO: 0033619; NES = 1.62, $p = 0.003$; Fig. 4B), "Membrane protein ectodomain proteolysis" (GO: 0006509; NES = 1.6, $p = 0.027$; Fig. 4C), and "Positive regulation of proteolysis involved in protein catabolic process" (GO: 1903052; NES = 1.6, $p < 0.0001$; Fig. 4D). Previous studies had connected the activity of Ca^{2+}-dependent calpain-type proteases to *rd1* retinal degeneration [55, 56] and we hypothesized that the neurodegenerative calpain-2 isoform [34] might be responsible for retinal cell death. Thus, we used the recently developed and highly specific calpain-2 inhibitor NA-184 [57] to treat *rd1* explant cultures. A dose-response curve for the effects of NA-184 was compiled (Figure S2F) and a concentration of 1 µM was chosen for further experiments. As before, in *wt* retina the numbers of TUNEL positive cells in the ONL were low (1.08% ± 0.44, $n = 4$) when compared with untreated *rd1* retina (4.8% ± 0.47, $n = 7$; Fig. 4E). NA-184 treatment significantly reduced *rd1* ONL TUNEL positive cells (3.55% ± 0.53, $n = 7$, $p < 0.01$; Fig. 4E), implying a causative involvement of calpain-2 in the degenerative process.

Calpain activity changes after interventions targeting intracellular Ca^{2+}

To further study how Ca^{2+} chelation, activity of Ca^{2+} permeable channels, and calpain-2 inhibition regulated overall calpain, we investigated calpain activity using a general in situ activity assay and immunolabelling for activated calpain-1 and calpain-2. Calpain activity and calpain-2 activation were rather low in *wt* retina when

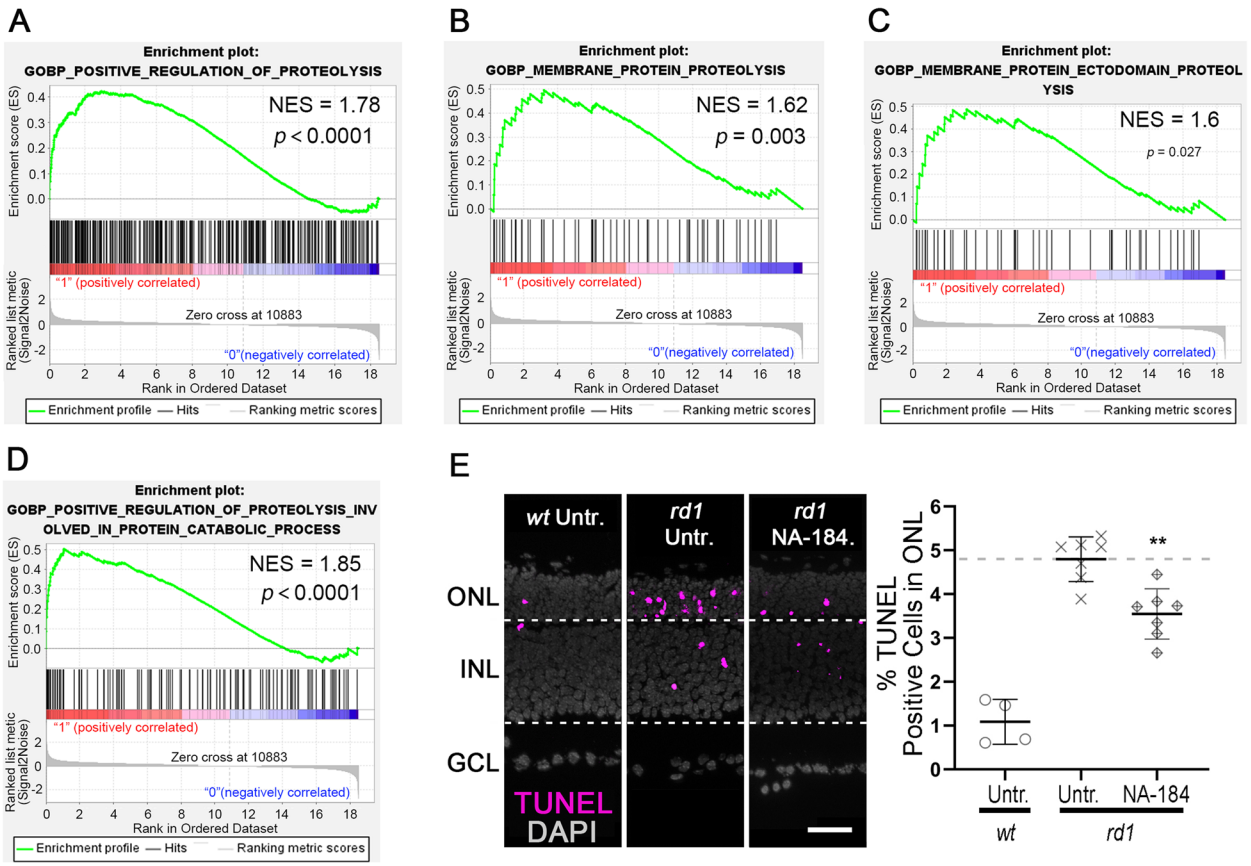

Fig. 4 Ca^{2+}-dependent proteolysis and calpain-2 are associated with *rd1* photoreceptor cell death. **A** Gene set enrichment analysis (GSEA) showing enrichment of differentially expressed genes (DEGs) in the biological process (BP) "Positive regulation of proteolysis" (GO: 0045862). **B** DEGs enriched in the BP "Membrane protein proteolysis" (GO: 0033619). **C** DEGs enriched in the BP "Membrane protein ectodomain proteolysis" (GO: 0006509). **D** DEGs enriched in the BP "Positive regulation of proteolysis involved in protein catabolic process" (GO:1903052). **E** TUNEL assay labelled dying cells (magenta) in wild-type (*wt*) and *rd1* retinal explant cultures. DAPI (grey) was used as nuclear counterstain. Untreated (Untr.) *wt* and *rd1* retina compared to retina treated with the calpain-2 selective inhibitor NA-184. Scatter plot shows percentage of TUNEL-positive cells in outer nuclear layer (ONL). Statistical comparison: Student's *t*-test performed between *rd1* Untr. and *rd1* NA-184. INL = inner nuclear layer, GCL = ganglion cell layer; scale bar = 50 µm

compared with *rd1* retina (Fig. 5A, C; Table S7A, C). BAPTA-AM significantly reduced both overall calpain activity and calpain-2 activation specifically (Fig. 5A, C; Table S7A, C; dose-response curve shown in Figure S2A). However, L-cis and CM4620 significantly increased both calpain activity and calpain-2 activation (Fig. 5A, C; Table S7A, C; dose response curve for CM4620 shown in Figure S2B). General calpain activity and calpain-2 activation were also significantly reduced after treatment with SN-6, D-cis, TTA-A2, and NA-184 (Fig. 5A, C; Table S7A, C). Dose-response curves for SN-6, TTA-A2, and NA-184 on *rd1* calpain activity are shown in Figure S2C, D, and F, respectively. Interestingly, DS5565 significantly reduced overall calpain activity, while it did not decrease calpain-2 activation, when compared to *rd1* control (Fig. 5A, C; Table S7A, C; dose response curve for DS5565 shown in Figure S2E).

In *wt* retina the numbers of calpain-1 activation in ONL were relatively similar when compared with that of *rd1* ($p > 0.05$; Fig. 5B and Table S7B). BAPTA-AM significantly increased the percentage of activated calpain-1 in *rd1* ONL, while L-cis did not (Fig. 5B; Table S7B). The number of activated calpain-1 positive cells in *rd1* ONL was significantly raised by CM4620 and SN-6, but not by D-cis, TTA-A2, and DS5565 (Fig. 5B; Table S7B). Interestingly, the calpain-2 inhibitor NA-184 significantly increased calpain-1 activation in *rd1* retina (Fig. 5B; Table S7B).

Relationships between activation of calpain-1, calpain-2, and cell death

To capture the presumed interactions between calpain-1, calpain-2, and cell death numerically, we applied Spearman's rank correlation coefficient analysis (Spearman analysis) to the corresponding datasets to assess the strength and direction of the monotonic relationship between variables [58]. Figure 6A illustrates that calpain-1 activation in *rd1* ONL correlated negatively with calpain-2 activation with R = -0.62 ($p < 0.01$), and similarly with cell death indicated by TUNEL positive cells (R = -0.65, $p < 0.0001$, Fig. 6B). Further, our hypothesis that calpain-1 activation may not be connected to cell death, while calpain-2 activation is, was supported by the fact that the ratio of calpain-2/calpain-1 was positively correlated with TUNEL ($R = 0.61$, $p < 0.01$, Fig. 6C), a similar association as would be expected for the effect of calpain-2 alone.

General trends in the relationships between calpain-1, calpain-2, and cell death were visualized in an alluvial diagram where the numbers of activated calpain-1, -2, and TUNEL positive cells in the ONL of the *rd1* control group were used as baseline (Fig. 6D). This representation suggests that in *rd1* retinal explant cultures treatment with BAPTA-AM, SN-6, D-cis, TTA-A2, DS5565, and NA-184 led to low calpain-2 activation in the ONL when compared to untreated (Fig. 6D). In contrast, L-cis and CM4620 treatments were related to high calpain-2 activation. Most of the low calpain-2 activation was linked to high calpain-1 activation and to a reduction of TUNEL positive cells in ONL (Fig. 6D). Taken together, the above data are in support of our hypothesis that calpain-1 activation was unrelated to cell death while calpain-2 activation was closely connected to it.

Effect of Ca^{2+} and calpain-2 on enzymatic activities of PARP and sirtuin

PARP was previously reported to be connected to photoreceptor cell death [4]. To dissect the relationship of Ca^{2+}, calpain, and PARP, we performed an in situ PARP activity assay and immunostaining for PAR, i.e. the product of PARP activity. While PARP activity and PAR-positive cells were infrequent in *wt* retina when compared with *rd1* (Fig. 7A, B; Table S8A, B), treatment with BAPTA-AM significantly reduced both PARP activity and PAR generation in *rd1* ONL (Fig. 7A, B; Table S8A, B; BAPTA-AM dose-response in Figure S2A), indicating

(See figure on next page.)

Fig. 5 Ca^{2+}-channel inhibitors differentially regulate general calpain activity, activation of calpain-1 and -2. **A** Calpain activity assay (blue) in wild-type (*wt*) and *rd1* retinal explant cultures, nuclear counterstain with ToPro (red). Untreated (Untr.) *wt* and *rd1* retina were compared to retina treated with BAPTA-AM, L-cis diltiazem, CM4620, SN-6, D-cis diltiazem, TTA-AS, DS5565, and NA-184. Scatter plot showing percent calpain activity positive cells in outer nuclear layer (ONL). Untr. *wt*: $n = 11$; Untr. *rd1*: 23; BAPTA *rd1*: 10; L-cis *rd1*: 6; CM4620 *rd1*: 5; SN-6 *rd1*: 9; D-cis *rd1*: 6; TTA-A2 *rd1*: 7; DS5565 *rd1*: 6; NA-184 *rd1*: 8. **B** Activated calpain-1 (cyan) immunostaining in *wt* and *rd1* retinal explant cultures with DAPI (grey) as nuclear counterstain. Untreated specimens were compared to retina treated with compounds as in A. Scatter plot showing percent ONL cells displaying calpain-1 activation. Untr. *wt*: $n = 7$; Untr. *rd1*: 17; BAPTA *rd1*: 9; L-cis *rd1*: 9; CM4620 *rd1*: 10; SN-6 *rd1*: 8; D-cis *rd1*: 10; TTA-A2 *rd1*: 8; DS5565 *rd1*: 8; NA-184 *rd1*: 9. **C** Activated calpain-2 (yellow) immunostaining in *rd1* and *wt* retinal explant cultures with DAPI (grey) as nuclear counterstain. Untreated specimens were compared to retina treated with compounds as in A. Scatter plot showing percent ONL cells displaying calpain-2 activation. Untr. *wt*: 10; Untr. *rd1*: 21; BAPTA *rd1*: 9; L-cis *rd1*: 9; CM4620 *rd1*: 10; SN-6 *rd1*: 7; D-cis *rd1*: 10; TTA-A2 *rd1*: 8; DS5565 *rd1*: 6; NA-184 *rd1*: 9. Note the significant elevation of calpain activity/calpain-2 activation caused by CNGC and CRAC inhibition. The opposite is observed for calpain-1 activation. Statistical testing: one-way ANOVA and Tukey's multiple comparison post hoc test; significance levels: * = $p < 0.05$; ** = $p < 0.01$; *** = $p < 0.001$; **** = $p < 0.0001$; error bars represent SD; INL = inner nuclear layer, GCL = ganglion cell layer; scale bar = 50 µm

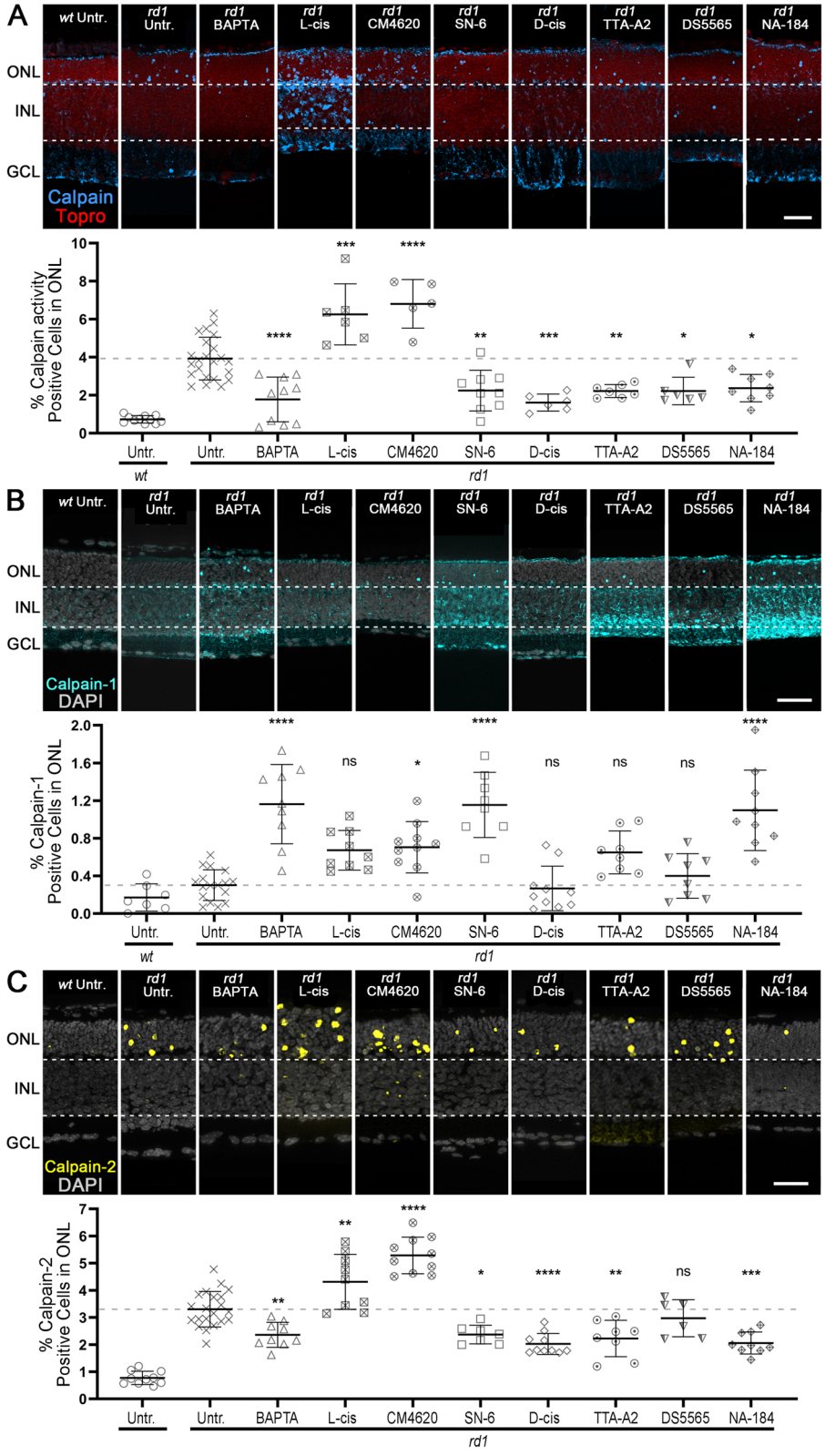

Fig. 5 (See legend on previous page.)

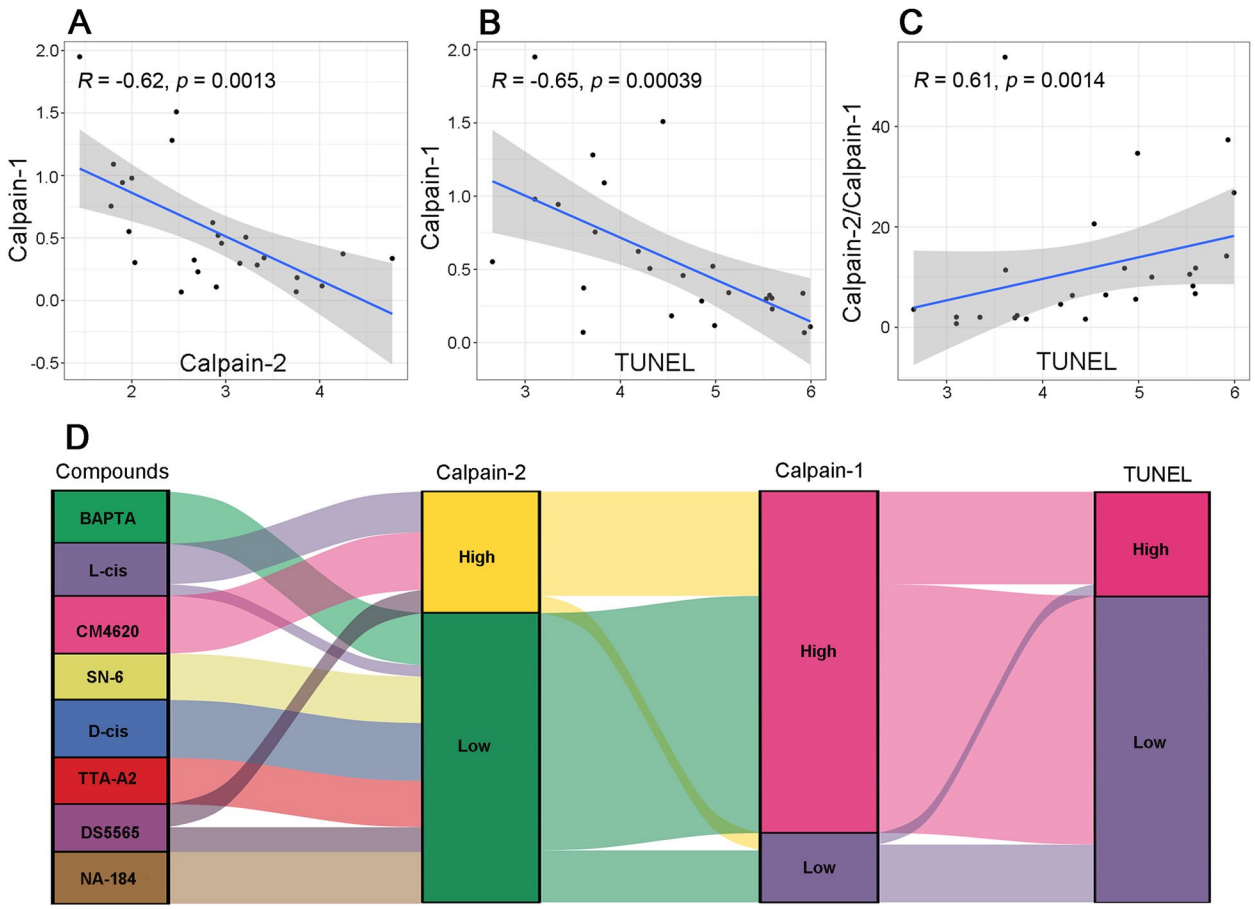

Fig. 6 Differential correlation of calpain-1 and calpain-2 to photoreceptor cell death. **A** Spearman analysis comparing the numbers of activated calpain-1 and calpain-2 in the outer nuclear layer (ONL) of untreated *rd1* retina and *rd1* retina treated with the calpain-2 inhibitor NA-184. **B** Spearman analysis between the numbers of activated calpain-1 and dying, TUNEL positive cells in untreated or NA-184 treated *rd1* ONL. **C** Spearman analysis between the ratio of calpain-2/calpain-1 and TUNEL positive cells in untreated or NA-184 treated *rd1* ONL. **D** Alluvial diagram showing the relationship between activated calpain-2 and calpain-1, as well as TUNEL positive cells in *rd1* ONL after treatment with BAPTA-AM, L-cis, CM4620, SN-6, D-cis, TTA-AS, DS5565, and NA-184

a Ca^{2+}-dependent mechanism for PARP activation. However, the Ca^{2+}-channel blockers L-cis and CM4620 significantly increased both PARP activity and PAR in *rd1* ONL (Fig. 7A, B; Table S8A, B; CM4620 dose-response in Figure S2B). In contrast, PARP activity and PAR positive cells in *rd1* ONL were significantly reduced after treatment with SN-6, D-cis, TTA-A2, and DS5565 (Fig. 7A, B; Table S8A, B; dose response curves for SN-6, TTA-A2, DS5565 shown in Figures S2C, D, and E, respectively). The calpain-2 inhibitor NA-184 neither decreased PARP

(See figure on next page.)

Fig. 7 Ca^{2+}-signalling affects PARP activity, PAR generation, and sirtuin activity. **A** PARP activity assay (green) was performed in *rd1* and wild-type (*wt*) retinal explant cultures, with DAPI (grey) as nuclear counterstain. Untreated (Untr.) *rd1* and *wt* retina were compared to *rd1* retina treated with BAPTA-AM, L-cis, CM4620, SN-6, D-cis, TTA-AS, DS5565, and NA-184. The scatter plot shows percentage of PARP activity positive cells in the outer nuclear layer (ONL). Untr. *wt*: $n = 11$; Untr. *rd1*: 24; BAPTA *rd1*: 10; L-cis *rd1*: 5; CM4620 *rd1*: 5; SN-6 *rd1*: 7; D-cis *rd1*: 10; TTA-A2 *rd1*: 6; DS5565 *rd1*: 6; NA-184 *rd1*: 8. **B** PAR staining (black) was performed in *rd1* and *wt* retinal explant cultures. Untreated *wt* and *rd1* retina were compared to drug-treated retina as in A. Untr. *wt*: $n = 6$; Untr. *rd1*: 17; BAPTA *rd1*: 7; L-cis *rd1*: 7; CM4620 *rd1*: 10; SN-6 *rd1*: 8; D-cis *rd1*: 8; TTA-A2 *rd1*: 8; DS5565 *rd1*: 8; NA-184 *rd1*: 9. **C** Sirtuin activity assay (white) was performed in *rd1* and *wt* retinal explant cultures. Untreated *rd1* and *wt* retina were compared to drug-treated retina as in A. Untr. *wt*: $n = 7$; Untr. *rd1*: 21; BAPTA *rd1*: 9; L-cis *rd1*: 9; CM4620 *rd1*: 10; SN-6 *rd1*: 8; D-cis *rd1*: 9; TTA-A2 *rd1*: 8; DS5565 *rd1*: 8; NA-184 *rd1*: 9. Statistical testing: one-way ANOVA with Tukey's multiple comparison post hoc test performed between *rd1* explant cultures. Error bars represent SD; ns = $p > 0.05$; * = $p < 0.05$; ** = $p < 0.01$; *** = $p < 0.001$; **** = $p < 0.0001$. INL = inner nuclear layer, GCL = ganglion cell layer; scale bar = 50 µm

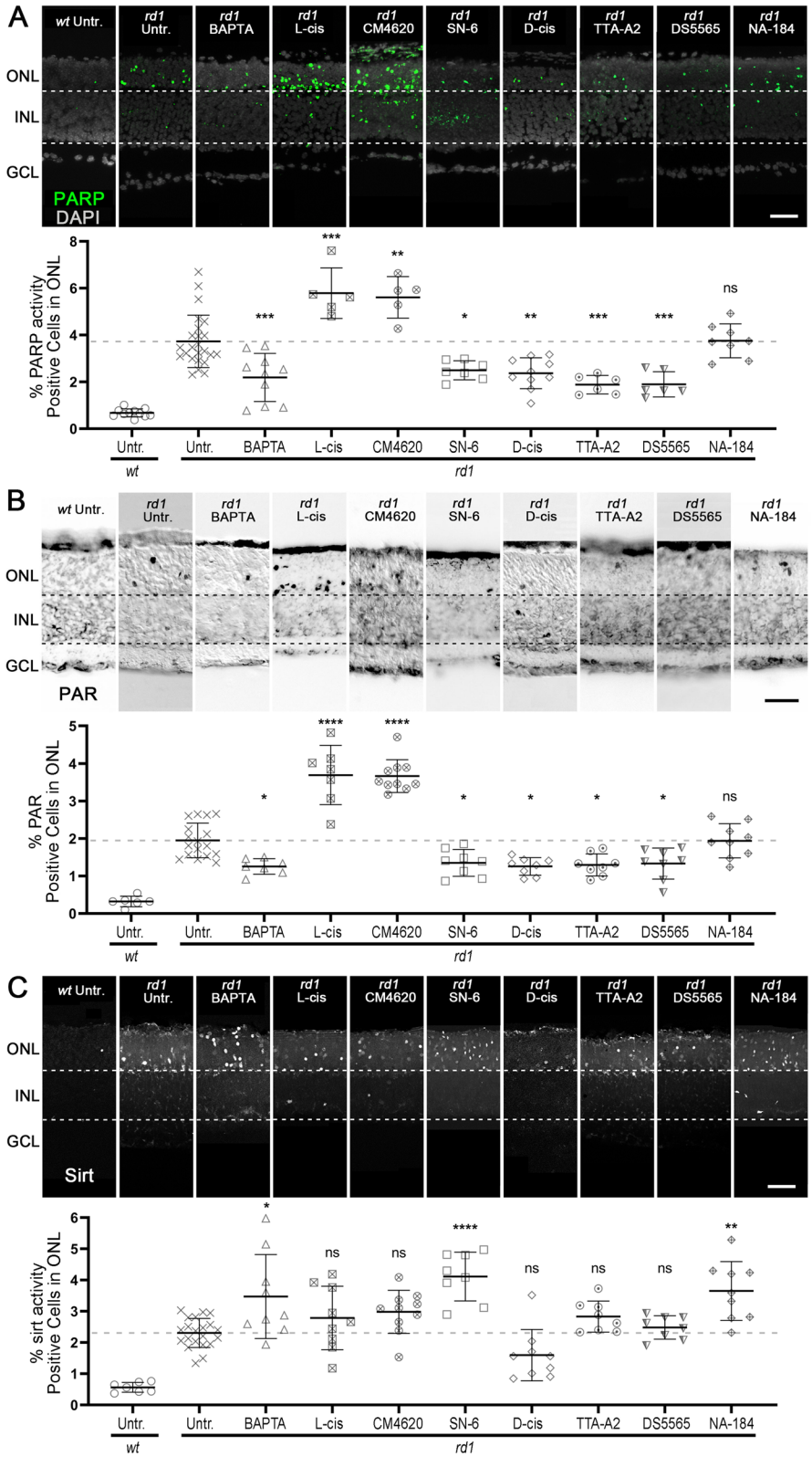

Fig. 7 (See legend on previous page.)

activity nor PAR generation in *rd1* ONL (Fig. 7A, B; Table S8A, B; NA-184 dose-response in Figure S2F).

The histone deacetylase (HDAC) sirtuin-1 (SIRT1) was suggested to be indirectly regulated by PARP-dependent consumption of NAD^+ [59]. Thus, we investigated sirtuin activity using an HDAC in situ activity assay based on deacetylation of a SIRT1 specific substrate. In *rd1* retina, the number of HDAC or sirtuin activity positive cells in the ONL was higher compared to *wt* control (Fig. 7C; Table S8C). BAPTA-AM further significantly increased sirtuin activity in *rd1* ONL (Fig. 7C; Table S8C). Treatment with L-cis and CM4620 did not change the numbers of sirtuin activity positive cells, as compared to untreated *rd1*, while sirtuin activity was increased by SN-6 (Fig. 7C; Table S8C). Sirtuin activity did not rise after treatment with D-cis, TTA-A2, and DS5565 (Fig. 7C; Table S8C), but unexpectedly, NA-184 significantly increased the percentage of sirtuin positive cells in *rd1* ONL (Fig. 7C; Table S8C).

Enzyme activity patterns are altered by changes in Ca^{2+} or by inhibition of calpain-2

To compare the various processes studied here with each other, we normalized the experimental data by linear scaling, such that the lowest values were set to zero while the highest values were set to one. In *wt* retina, all TUNEL staining and all enzyme activity markers were generally low when compared with the untreated *rd1* group (Fig. 8A). In untreated *rd1*, the number of ONL cells showing calpain-1 activation was lower than calpain activity, calpain-2 activation, PARP activity, PAR positive cells, and sirtuin activity (Fig. 8A). Photoreceptor degeneration was significantly reduced by treatments with BAPTA-AM, SN-6, TTA-A2, and NA-184, while calpain-1 activation and sirtuin activity were relatively high, compared to other markers (Fig. 8A). In contrast, the treatments with L-cis and CM4620, which increased photoreceptor death, increased calpain activity, calpain-2 activation, PARP activity, and PAR-positive cells more than calpain-1 activation and sirtuin activity (Fig. 8A). In the D-cis and DS5565 treated groups, which did not affect photoreceptor viability, calpain-1 activation in ONL was generally lower than calpain-2 activation (Fig. 8A). Taken together, the activity patterns observed may constitute enzymatic signatures characteristic for either retinal degeneration or protection.

To numerically capture these presumed activity patterns triggered by alterations in Ca^{2+}-influx, we performed a Spearman analysis (Fig. 8B). This analysis excluded data from the NA-184 treatment since this calpain inhibitor would not per se change Ca^{2+}-influx. General calpain activity and calpain-2 activation was positively correlated with PARP activity and PAR ($R > 0.7$, $p < 0.0001$). Calpain-1 activation and sirtuin activity were also positively correlated with each other ($R > 0.6$, $p < 0.0001$). A radar plot was used to show the relationship of cell death and enzymatic signatures after Spearman analysis (Fig. 8C). This illustrated that TUNEL positive cells in *rd1* ONL were positively correlated with calpain activity, calpain-2 activation, PARP activity and PAR ($R > 0.7$, $p < 0.0001$, Fig. 8C). However, TUNEL positive cells were anti-correlated with sirtuin activity and calpain-1 activation. Taken together, these analyses suggest that calpain-1 activation and sirtuin activity were associated with photoreceptor survival, as opposed to general calpain activity, calpain-2, PARP, and PAR, which were strongly connected to cell death.

Discussion

Ca^{2+} overload mediated by CNGC and VGCC has repeatedly been connected to cGMP-induced photoreceptor death in IRD models [15, 60, 61]. However, a number of studies using inhibitors of Ca^{2+}-permeable channels have reported contradictory effects [62, 63], such that the precise role of Ca^{2+} in photoreceptor degeneration is still unclear. Our initial bioinformatics analysis provided insights into the regulation of Ca^{2+}-related genes connected to retinal degeneration. However, since gene expression along does not necessarily reflect the actual protein expression and protein functioning, we then used pharmacological experiments to confirm perturbations of intracellular Ca^{2+} in the diseased retina. homeostasis may cause photoreceptor degeneration, and that blocking Ca^{2+}-influx may be neuroprotective. More specifically, our data suggest that Ca^{2+}-permeable channels, T-type VGCC, and possibly also NCX, may serve as therapeutic

(See figure on next page.)

Fig. 8 Enzymatic signatures for *rd1* photoreceptor degeneration and Spearman analysis. **A** Comparison of enzymatic markers across different experimental treatments. Normalized cell numbers positive for TUNEL (magenta), calpain activity (calpain, blue), activated calpain-2 (yellow), PARP activity (PARP, green), PAR (black), activated calpain-1 (cyan), and sirtuin (Sirt) activity (white). **B** Spearman analysis of enzymatic markers in photoreceptors (calpain activity, calpain-1, calpain-2, PARP activity, PAR, Sirtuin). The asterisks in circles show statistical significance, numbers in squares present the *R*. **C** Radar plot for Spearman analysis revealing the correlation between different enzymatic markers and the TUNEL assay. Note that while cell death (TUNEL) was strongly associated with general calpain activity, calpain-2 activation, PARP activity, and PAR, it was negatively correlated with calpain-1 activation and Sirtuin activity

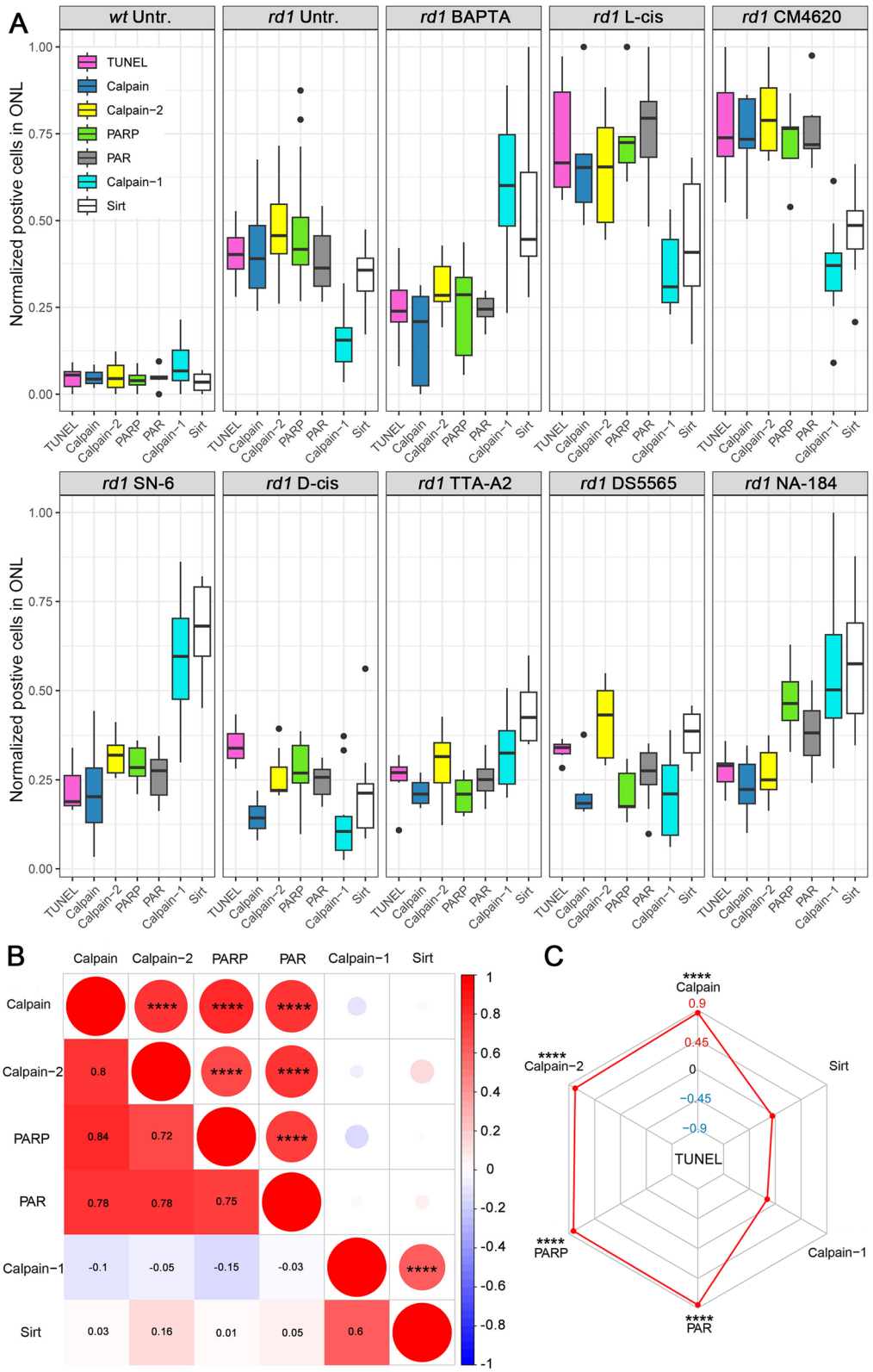

Fig. 8 (See legend on previous page.)

targets for the treatment of IRDs (Fig. 9). Additionally, the activity of the Ca^{2+}-activated proteolytic enzyme calpain-1, in contrast to calpain-2, was linked to lower cell death rates. Consequently, an inhibition of calpain-2 turned out to be neuroprotective. Overall, our study indicates that both substantial positive or negative deviations of intracellular Ca^{2+} levels may endanger photoreceptor viability.

Ca^{2+} homeostasis is critical for the survival of retinal photoreceptors

In different cell types, the second messenger Ca^{2+} is involved in the regulation of a diverse range of cellular processes, including fertilization, metabolism, transcription, and cell death [64]. This diversity of Ca^{2+}-signalling related processes requires a precise control of intracellular Ca^{2+} levels, which in a healthy cell are maintained at below 100 nM vs. extracellular levels exceeding 2 mM [64]. In photoreceptors, the over-activation of CNGC caused by high intracellular cGMP levels leads to an influx of Na^+ and Ca^{2+}, depolarizing the cell and activating VGCC, causing further Ca^{2+} influx [5, 61]. However, whether Ca^{2+} is responsible for photoreceptor degeneration is debated, as some reports indicate that blocking Ca^{2+}-permeable channels may be neuroprotective [18, 19, 65], while other studies propose the opposite [20, 21]. Our bioinformatic analysis of RNA-seq data obtained at the peak of *rd1* photoreceptor cell death (P13) revealed more than 80 DEGs associated with Ca^{2+}. GSEA analysis and GO enrichment identified Ca^{2+}-related DEGs

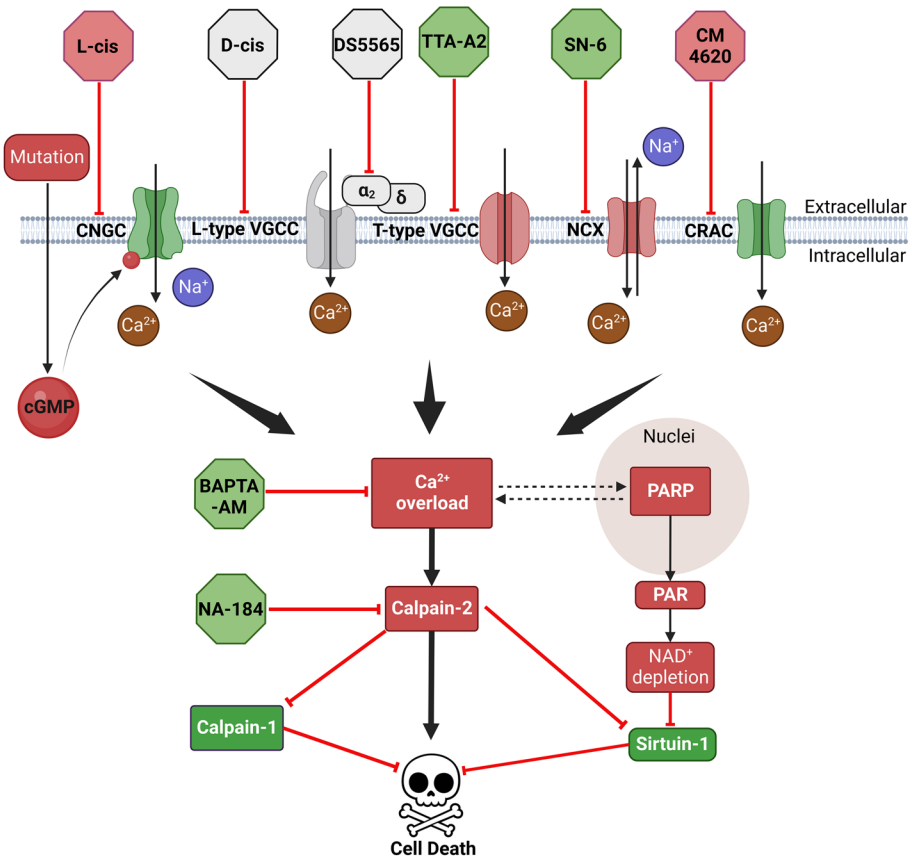

Fig. 9 Experimental interventions and their relation to Ca^{2+} signalling in cGMP-dependent *rd1* degeneration. In *rd1* photoreceptors, the *Pde6b* mutation induces cGMP accumulation, which activates cyclic-nucleotide-gated channels (CNGC), leading to Na^+ and Ca^{2+} influx. CNGC-dependent depolarization activates voltage-gated Ca^{2+} channel (VGCC) and may reverse directionality of Na^+/Ca^{2+} exchanger (NCX), both leading to more Ca^{2+}-influx. Additional Ca^{2+}-influx may be mediated by Ca^{2+} release activated channel (CRAC). All these Ca^{2+} permeable channels may contribute to intracellular Ca^{2+} overload, which, in turn, may activate calpain-2 directly and poly(ADP-ribose)-polymerase (PARP) indirectly. On the one hand, over-activated calpain-2 increases proteolysis of neuroprotective calpain-1. On the other hand, Ca^{2+}-dependent activation of PARP may positively feedback on Ca^{2+}-influx via NAD^+ depletion, which may reduce the protective activity of NAD^+-dependent sirtuins. Eventually, the activities of calpain-2 and PARP, triggered by high intracellular Ca^{2+}-levels promote photoreceptor cell death. The drugs used in this study and their targets are indicated. Red colour indicates destructive processes and drugs, while green labelled proteins and compounds promote photoreceptor survival, grey indicates absence of a clear beneficial or destructive effect

associated with four pathways linked to proteolysis. Since at P13 the *rd1* retina loses mainly rod photoreceptors [14], we then used scRNA-seq to focus on Ca^{2+}-related pathways in photoreceptors. DEGs were enriched in Ca^{2+}-related GO terms in both rods and cones, however, remarkably, rods displayed gene regulation in more Ca^{2+}-related GO terms than cones. The well-studied membrane permeable Ca^{2+} chelator, BAPTA-AM, preserved photoreceptor viability, providing strong evidence for a contribution of excessive Ca^{2+}-levels to *rd1* rod degeneration. However, exceedingly low Ca^{2+} levels are also known to trigger cell death [66]. In line with this, BAPTA-AM increased the numbers of dying, TUNEL positive cells in *wt* retina and strongly increased cell death in *rd1*Cngb1*$^{-/-}$ double-mutant retina. Together, these findings demonstrate that both exceedingly high Ca^{2+} levels and a depletion of intracellular Ca^{2+} can lead to retinal degeneration [67]. The key question that remains is which Ca^{2+}-permeable channel(s) may be responsible for excessive Ca^{2+}-influx.

CNGC and CRAC activity does not promote *rd1* degeneration

In the present study, we investigated the roles of CNGC, CRAC, NCX, and VGCC in photoreceptor cell death (Fig. 9). CNGC is activated by high cGMP, linking it to the *rd1* mutation in PDE6. The CNGC gene family comprises six members (*CNGA1-4*, *CNGB1* and *CNGB3*), of which CNGA1 and CNGB1 are expressed by rods, while CNGA3 and CNGB3 are expressed in cones [68]. In the whole retina RNA-seq data *Cnga1* appeared to be down-regulated, while the scRNA-seq showed it as up-regulated in rod photoreceptors. This discrepancy may have been caused by the ongoing photoreceptor degeneration since in P13 *rd1* retina a number of rod photoreceptors have been lost already compared to their P13 wt counterparts [14]. However, the inhibition of CNGC by L-cis-diltiazem accelerated photoreceptor cell death, in line with previous research [20], but in apparent contradiction with data obtained in *rd1*Cngb1*$^{-/-}$ double-mutant mice [19]. However, the *rd1*Cngb1*$^{-/-}$ double-mutant mice still retain residual CNGC activity and Ca^{2+}-influx through homomeric CNGA1 channels [69]. L-cis-diltiazem treatment will abolish even this residual Ca^{2+}-influx, probably leading to cell death triggered by too low intracellular Ca^{2+}.

CRAC activity has previously been connected to cell death and inhibition of CRAC has been shown to increase cell viability [70]. CaMK2 may potentiate SOCE and CRAC activity *via* enhancing Stim1 aggregation and interaction with Orai [53]. In *Pde6b*-mutant mice, the *Camk2g* gene was found to be up-regulated in the present and in previous studies [71]. However, the *Camk2d* gene displayed a down-regulation in to the bulk RNA-seq dataset, which warranted an independent confirmation as to whether CRAC contributed to Ca^{2+} overload during *rd1* retinal cell death. Selective CRAC inhibition with CM4620 triggered photoreceptor degeneration in *wt* retina and increased photoreceptor death even further in *rd1* retina, indicating that contrary to our expectations CRAC-mediated Ca^{2+}-influx was essential for photoreceptor survival.

Taken together, our data indicates that the activity of CNGC and CRAC Ca^{2+}-permeable channels appears to be protective rather than destructive, and thus neither of these is linked to *rd1* photoreceptor degeneration. We note that these results may have been influenced by our use of early post-natal retina, in which photoreceptors and their outer segments are not yet fully developed. However, given the marked detrimental effects of CNGC and CRAC inhibitors, it seems unlikely that this outcome would change in more mature retina.

T-type VGCC and NCX contribute to Ca^{2+} overload and *rd1* photoreceptor cell death

Apart from CNGC and CRAC, we also investigated the importance of different VGCC-types and NCX for *rd1* degeneration. NCX is a bi-directional regulator of cytosolic Ca^{2+}, capable of mediating both Ca^{2+} influx and Ca^{2+} efflux. NCX inhibition bestows resistance to retinal damage induced by *N*-methyl-D-aspartate (NMDA) and high intraocular pressure [72]. In our hands, the NCX inhibitor SN-6 [73] reduced calpain activity and prolonged *rd1* photoreceptor viability, yet it increased cell death in the *wt* situation. This suggests a reversal of NCX directionality in the two different genotypes, possibly caused by high intracellular Na^{+} levels [52] and membrane depolarization [24]. Thus, cGMP-dependent over-activation of CNGC may have reversed NCX in *rd1* rod photoreceptors. Surprisingly, while BAPTA-AM led to photoreceptor cell death in *rd1*Cngb1*$^{-/-}$ retina, perhaps due to Ca^{2+} depletion, NCX inhibition in the *rd1*Cngb1*$^{-/-}$ situation attenuated retinal degeneration, indicating that NCX is in forward mode when CNGC activity is low. However, neither BAPTA-AM nor SN-6 preserved the outer retina in the long-term, implying that other mechanisms, such as those triggered by cGMP-dependent protein kinase G (PKG) may promote retinal degeneration independent of elevated Ca^{2+} [74, 75].

VGCC is activated by membrane depolarization, allowing Ca^{2+} entry into the cells [76]. VGCC consists of four non-covalently associated subunits: α_1 (L-type and T-type VGCC), β, $\alpha_2\delta$, and γ [77]. In *rd1* photoreceptors, VGCC may indirectly be activated by cGMP-induced over-activation of CNGC [61]. Hence, D-cis-diltiazem [78], DS5565 [79], and TTA-A2 [80] were used to block

different VGCC types. D-cis-diltiazem did not prevent retinal degeneration, consistent with previous literature [21, 81, 82]. Interestingly, L-type VGCC genes (*Cacna1s* and *Cacna1f*) were shown up- and down-regulated respectively, suggesting there could be variable effects within different L-type VGCC isoforms. Furthermore, while we observed an up-regulation of genes coding for the $\alpha_2\delta$ subunits of VGCC in *rd1* rods, treatment with the $\alpha_2\delta$ subunit VGCC ligand DS5565 did not protect *rd1* photoreceptors either. However, DS5565 reduced calpain activity, indicating that the $\alpha_2\delta$ subunit was effectively regulating intracellular Ca^{2+} levels. Our data RNA-seq and scRNA-seq also indicate a differential regulation of the β subunit of VGCC (*Cacnb2*), which, however, does not seem to be related to an increased therapeutic response to VGCC inhibition.

Unexpectedly, it was the inhibition of T-type VGCC that significantly attenuated photoreceptor cell death. This is surprising since T-type channels are generally thought to open at relatively negative membrane potentials of around −40 to -80 mV, as opposed to L-type channels which may open already at -20 mV [83]. In photoreceptors the resting potential is approx. -40 mV and the membrane potential would reach −70 mV only during light-induced photoreceptor hyperpolarisation [84]. Thus, in *rd1* photoreceptors, which cannot be hyperpolarized by light due to PDE6 dysfunction, one would assume that L-type VGCC rather than T-type should carry most of the Ca^{2+}-currents. However, we cannot exclude the possibility that T-type channels change their properties to become permeable at less negative membrane potential, or that the *rd1* photoreceptor membrane potential shifts to more negative values.

Overall, our data suggest T-type VGCC and NCX contribute to *rd1* retinal degeneration. One may speculate that in the initial phases of an individual photoreceptor´s demise, the membrane potential is still maintained at sufficiently negative values, allowing for an opening of T-type channels and Ca^{2+}-influx. Eventually, however, the cell may no longer be able to keep its membrane potential and becomes depolarized, so much so that NCX reverses its direction and turns into a net importer of Ca^{2+}. This idea of two different stages in the dysregulation of photoreceptor Ca^{2+}-levels may also help to understand why NCX inhibition did not afford long-term protection. While the exact mechanism remains to be clarified, our data importantly highlights T-type VGCC as a potential target for therapeutic [84] intervention.

Calpain-2 causes photoreceptor cell death and negatively regulates calpain-1

High levels of intracellular Ca^{2+} will activate calpain-type proteases and calpain activation may be connected to CNGC activity [19, 85]. Calpain consist of a family of Ca^{2+}-activated neutral cysteine proteinase involved in a large number of cellular processes [34, 86]. Originally, the calpain proteolytic system was reported to consist of three different proteins: calpain-1 (or μ-calpain, activated at μM Ca^{2+} concentrations) and calpain-2 (or m-calpain, activated at mM Ca^{2+} concentrations), as well as their endogenous inhibitor, calpastatin [86]. Recent evidence indicates that calpain-1 and calpain-2 play opposite roles, with calpain-1 being neuroprotective while calpain-2 promotes neurodegeneration [34]. We previously found that in *rd1* mice, activated calpain-2 was increased rather than calpain-1 [56], and the current GSEA analysis indicated a positive regulation of proteolytic pathways. Thus, we assumed that calpain-2, as part of the proteolytic processes induced by Ca^{2+} [87], led to retinal degeneration. Therefore, we treated *rd1* retina with the calpain-2 specific inhibitor NA-184 [57]. This caused a significant decrease in the numbers of TUNEL positive cells in the ONL, highlighting the role of calpain-2 in photoreceptor cell death. On the other hand, calpain-1 activation was decreased in situations where calpain-2 activation was high, possibly due to calpain-2-dependent cleavage of calpain-1´s protease core domain 1 [88]. Accordingly, NA-184 treatment also increased calpain-1 activation. These findings extend one of our previous studies where we found the general calpain inhibitor calpastatin peptide to protect photoreceptors in vitro and in vivo [89]. Yet, since calpastatin peptide inhibits both calpain-1 and −2, the beneficial effects of calpain-2 inhibition may have been partly offset by the additional calpain-1 inhibition. Taken together, we found calpain-2 activation to be related to photoreceptor cell death, and this was associated with decreased calpain-1 activation.

It is important to note that our general calpain activity assay does not discriminate between specific calpain isoforms and that also isoforms other than calpain-2 could be involved in photoreceptor degeneration. A candidate isoform may be calpain-5 which was shown to be expressed in the retina [90] and found to be involved in inherited forms of uveitis [91]. Calpain overactivation may be relevant also for a variety of other retinal neurodegenerative diseases, including neovascular inflammatory vitreoretinopathy (NIV), diabetic retinopathy (DR), uveitis, glaucoma, and cataractogenesis [92]. Specifically, calpain-2 has been connected to NIV, cataractogenesis, and glaucoma, while calpain-5 was associated with NIV and uveitis [92, 93]. Whatever the case, inhibition of calpain-2 and/or -5 could provide therapeutical benefit in these ocular diseases.

Ca^{2+} differentially regulates PARP and sirtuin activity

PARP and HDAC activity were previously connected to *rd1* degeneration and to Ca^{2+}-signalling [85, 94, 95]. PARP is a DNA repair enzyme, which catalyses the polymerization of ADP-ribose units – derived from the ADP donor NAD^+ – resulting in the attachment of either linear or branched PAR polymers to itself or other target proteins [96]. However, excessive PARP activity may drive a specific form of cell death, termed PARthanatos [97], which has also been connected to in retinal degeneration [4]. Accordingly, in certain IRD animal models, PARP inhibition was found to be neuroprotective [16, 98]. In line with previous literature [99, 100], the inhibition of Ca^{2+} -permeable channels reduced PARP activity and PAR generation in *rd1* explants, suggesting that Ca^{2+} regulated PARP activity. However, it is yet unclear how Ca^{2+} produces PARP over-activation. The specific calpain-2 inhibitor, NA-184, did not reduce PARP activity in *rd1* explants, suggesting that Ca^{2+} controls PARP activity independently of calpain-2 activity [16]. Instead the PARP activity observed may be caused by high levels of Ca^{2+} stimulating respiratory chain activity and leading to higher amounts of reactive oxygen species [101]. This in turn could produce oxidative DNA damage and trigger PARP hyper-activation [96, 102].

HDACs catalyse the removal of acetyl groups from lysine residues of both histone and nonhistone proteins [103]. HDACs are divided into zinc-dependent HDACs, and sirtuins, a family of NAD^+-dependent HDACs [103]. As PARP is a main consumer of NAD^+ [104], sirtuin activity can be regulated by PARP according to the NAD^+ levels [105]. The Sirtuin-1 protein is suggested to be protective in neurons [106]. While we observed decreased PARP activity after most of our experimental interventions, sirtuin activity was increased after treatment with BAPTA-AM and the NCX inhibitor SN-6, suggesting that the resultant decrease in PARP activity may relieve the NAD^+ shortage induced by PARP. Interestingly, calpain-2 inhibition also increased sirtuin activity without affecting PARP activity. However, currently there is no evidence indicating that calpain-2 cleaves HDACs. Still, HDACs may regulate calpain-2 activation indirectly *via* epigenetically increasing calpastatin expression [107]. Calpain may also influence mitochondrial biogenesis, as calpain plays a detrimental role upstream of the peroxisome proliferator-activated receptor γ (PPARγ) coactivator-1α (PGC-1α) pathway [108], which regulates the transcription of numerous nuclear-encoded mitochondrial genes [109] and is a key driver of mitochondrial biogenesis [110]. Thus, it appears possible that calpain-2 inhibition may improve *rd1* photoreceptor energy metabolism.

Conclusion

In IRD research, the role of Ca^{2+}-signalling in disease pathogenesis has remained controversial for a long period of time. The novel results presented here indicate that Ca^{2+}-signalling may have both beneficial and detrimental effects in *rd1* photoreceptors, depending on the source of Ca^{2+} and probably its intracellular localization. More specifically, inhibition of CNGC and CRAC accelerated cell death, while Ca^{2+} chelation, as well as inhibition of NCX and T-type VGCC increased photoreceptor viability. A selective inhibition of calpain-2 improved photoreceptor viability as well, while, remarkably, activation of calpain-1 and sirtuin-type HDAC was linked to photoreceptor survival. In contrast, general calpain activity and activity of PARP were found to be destructive. While our results propose T-type VGCC and calpain-2 as therapeutic targets for IRD treatment (Fig. 9), a careful context- and genotype-specific evaluation appears indicated as suggested, for instance, by the opposing results obtained in *rd1* single-mutant and *rd1*Cngb1*$^{-/-}$ double-mutant retina. In perspective, our study illustrates the complexity of Ca^{2+}-signalling during photoreceptor degeneration and highlights the need for additional work to further delineate destructive and protective pathways to promote the rational development of new therapeutic approaches for IRD and related retinal diseases.

Supplementary Information

The online version contains supplementary material available at https://doi.org/10.1186/s12964-023-01391-y.

Additional file 1: Figure S1. Photoreceptor scRNA-Seq and effects of interventions targeting photoreceptor Ca^{2+}-permeable channels. A) Differentially expressed genes (DEGs) in *rd1* rod photoreceptors at post-natal day (P)13. B) DEGs in *rd1* cone photoreceptors at P13. C) Effect of 10 µM BAPTA-AM and 40 µM SN-6 treatments on *rd1*Cngb1*$^{-/-}$ retinal cultures. TUNEL and the outer nuclear layer (ONL) thickness in treated retinas compared to Untr. *rd1* specimens. D) Different interventions targeting Ca^{2+}-permeable channels in *wt* retinal explant cultures. Scatter plots show percentage of TUNEL positive cells in ONL. Scale bars in C = 50 µM. Statistical significance was assessed using one-way ANOVA and Tukey's multiple comparison *post hoc* test. Untr.: *n*=8 retinal explants from different animals; BAPTA: 5; L-cis: 4; CM4620: 6; SN-6: 7; D-cis: 6; TTA-A2: 3; DS5565: 4. **Figure S2.** Dose-response curves for BAPTA-AM, CM 4620, SN-6, TTA-A2, DS5565, and NA-184. A) Dose-response curve for BAPTA-AM in *rd1* explant cultures. In the outer nuclear layer (ONL), 10, 25, and 50 µM BAPTA-AM significantly reduced calpain activity, PARP activity, and cell death as detected *via* the TUNEL assay. B) Different concentrations of CM4620 were tested in *rd1* explant cultures. In the ONL, at concentrations of 20 µM and 60 µM, CM4620 significantly increased ONL calpain activity, PARP activity, and cell death, as assessed by the TUNEL assay. C) Dose-response for SN-6 in *rd1* explant cultures. 20 µM and 40 µM SN-6 significantly reduced calpain activity, PARP activity, and cell death (TUNEL) in the ONL. B) Different concentrations of TTA-A2 were tested in *rd1* explant cultures. In ONL, 10 µM TTA-A2 significantly reduced calpain activity, PARP activity, and cell death as assessed with the TUNEL assay. C) Dose-response for DS5565 in *rd1* explant cultures. 15 µM DS5565 significantly reduced calpain activity, PARP activity, but not cell death (TUNEL) in the ONL. D) Dose-response for NA-184 in *rd1* explant cultures. At concentrations of 1 µM and 10 µM NA-184 significantly reduced ONL calpain activity

and cell death (TUNEL) but did not decrease PARP activity. Statistical significance was assessed using one-way ANOVA and Tukey's multiple comparison post hoc test. **Figure S3.** Effects of interventions targeting photoreceptor Ca^{2+}-permeable channels, bioinformatic analysis, and retinal NCX expression. A) Long-term treatment from P5 to P23, with 10 µM BAPTA and 40 µM SN-6, in *rd1* explant cultures, compared to untreated (Untr.) wild-type (*wt*) and *rd1* specimens. B) Balloon plot showing time-dependent expression changes (post-natal day (P) 11 to P17) of cyclic nucleotide-gated channel (CNGC), Ca^{2+}-release activated channel (CRAC), Na^{+}/Ca^{2+} exchanger (NCX), and voltage-gated Ca^{2+} channel (VGCC) in *rd1* cone photoreceptors. C) Analysis of Ca^{2+}/calmodulin-dependent protein kinase II (CaMK2) gene expression during *rd1* photoreceptor degeneration. D) Immunostaining of Na^{+}/Ca^{2+} exchanger (NCX) family. NCX1 was expressed in both inner and outer retina, while NCX2 and NCX3 were not detected. Occasional staining for NCX3 in retinal blood vessels relates to the use of anti-mouse secondary antibodies and (false positive) detection of IgG. **Supplemental Table 1.** Differentially expressed genes (DEGs) in *rd1* whole retina at post-natal day (P)13. **Supplemental Table 2.** Differentially expressed genes (DEGs) in *rd1* rod photoreceptors at post-natal day (P)13. **Supplemental Table 3.** Differentially expressed genes (DEGs) in *rd1* cone photoreceptors at post-natal day (P)13. **Supplemental Table 4.** Ca^{2+}-related GO terms in rod photoreceptors. **Supplemental Table 5.** Ca^{2+}-related GO terms in cone photoreceptors. **Supplemental Table 6.** Quantification of TUNEL positive, dying cells in outer nuclear layer (ONL). **Supplemental Table 7.** Quantification of cells positive for calpain activity/activation in outer nuclear layer (ONL). **Supplemental Table 8.** Quantification of cells positive for PARP activity, PAR accumulation, and sirtuin activity in outer nuclear layer (ONL).

Acknowledgements
The authors would like to thank Michel Baudry (CDM, Western University of Health Sciences, Pomona, CA) for providing NA-184, and editing the manuscript. We thank Norman Rieger (Institute for Ophthalmic Research, Eberhard-Karls-Universität Tübingen) for excellent technical assistance.

Authors' contributions
Conceptualization, J.Y. and F.P.-D.; methodology, J.Y., L.W., X.H., Y.D., K.J. and Z.H.; software, Q-L.Y., Q-X.Y. and J.Y.; validation, J.Y. and L.W.; formal analysis, Q-L.Y. and Q-X.Y.; investigation, J.Y. and L.W; data curation, J.Y.; writing-original draft preparation, J.Y., L.W. and Q-L.Y.; writing—review and editing, F.P-D. and M.S.; visualization, J.Y. and Q-L.Y.; supervision, F.P-D.; project administration, F.P-D.; funding acquisition, F.P-D. All authors have read and agreed to the published version of the manuscript.

Funding
Open Access funding enabled and organized by Projekt DEAL. This research was supported by grants from Charlotte and Tistou Kerstan foundation, the Zinke Heritage foundation, the Medical Leading Talents Training Program of Yunnan Provincial Health Commission (L-2019029), Yunnan Science and Technology Plan Progect (No.202105AF150067), the Joint Project of Yunnan Provincial Department of Science and Technology, Kunming Medical University on Applied Basic Research (No.202301AY070001-184), the Scientific Research Fund of Education Department of Yunnan Province (No. 2023J0050), Key Project of Yunnan Fundamental Research Projects (202301AS070046), and the National Natural Science Foundation of China (No.82360604). We acknowledge support from the Open Access Publication Fund of the University of Tübingen.

Declarations

Competing interests
The authors declare no competing interests.

Author details
[1]Yunnan Eye Institute & Key Laboratory of Yunnan Province, Yunnan Eye Disease Clinical Medical Center, Affiliated Hospital of Yunnan University, Yunnan University, 176 Qingnian, Kunming 650021, China. [2]Cell Death Mechanism Group, Institute for Ophthalmic Research, University of Tübingen, Tübingen 72076, Germany. [3]Graduate Training Centre of Neuroscience, University of Tübingen, Tübingen 72076, Germany. [4]The Third Affiliated Hospital of Kunming Medical University &Yunnan Cancer Hospital, Kunming, Yunnan 650118, China. [5]High-resolution Functional Imaging and Test Group, Institute for Ophthalmic Research, University of Tübingen, Tübingen 72076, Germany. [6]Division of Ocular Neurodegeneration, Institute for Ophthalmic Research, University of Tübingen, Tübingen 72076, Germany.

Received: 29 September 2023 Accepted: 9 November 2023
Published online: 01 February 2024

References

1. Botto C, et al. Early and late stage gene therapy interventions for inherited retinal degenerations. Prog Retin Eye Res. 2021;86:100975.
2. Verbakel SK, et al. Non-syndromic retinitis pigmentosa. Prog Retin Eye Res. 2018;66:157–86.
3. Arango-Gonzalez B, et al. Identification of a common non-apoptotic cell death mechanism in hereditary retinal degeneration. PLoS One. 2014;9(11):e112142.
4. Yan J, et al. Programmed non-apoptotic cell death in hereditary retinal degeneration: crosstalk between cGMP-dependent pathways and PARthanatos? Int J Mol Sci. 2021;22(19):10567.
5. Power M, et al. Cellular mechanisms of hereditary photoreceptor degeneration–focus on cGMP. Prog Retin Eye Res. 2020;74:100772.
6. Waldner D, Bech-Hansen N, Stell W. Channeling vision: CaV1. 4—a critical link in retinal signal transmission. Biomed Res Int. 2018;2018:7272630.
7. Haines DE. Fundamental neuroscience for Basic and clinical applications E-Book: with student consult online Access. Pennsylvania: Elsevier Health Sciences; 2012.
8. Ingram NT, Sampath AP, Fain GL. Membrane conductances of mouse cone photoreceptors. J Gen Physiol. 2020;152(3):e201912520.
9. Tolone A, et al. Pathomechanisms of inherited retinal degeneration and perspectives for neuroprotection. Cold Spring Harb Perspect Med. 2022;1:a041310.
10. Keeler CE. The inheritance of a retinal abnormality in white mice. Proc Natl Acad Sci. 1924;10(7):329–33.
11. Kalloniatis M, et al. Using the rd1 mouse to understand functional and anatomical retinal remodelling and treatment implications in retinitis pigmentosa: a review. Exp Eye Res. 2016;150:106–21.
12. Han J, et al. The history and role of naturally occurring mouse models with Pde6b mutations. Mol Vis. 2013;19:2579.
13. Paquet-Durand F, et al. PKG activity causes photoreceptor cell death in two retinitis pigmentosa models. J Neurochem. 2009;108(3):796–810.
14. Sancho-Pelluz J, et al. Photoreceptor cell death mechanisms in inherited retinal degeneration. Mol Neurobiol. 2008;38(3):253–69.
15. Frasson M, et al. Retinitis pigmentosa: rod photoreceptor rescue by a calcium-channel blocker in the rd mouse. Nat Med. 1999;5(10):1183–7.
16. Yan J, et al. Inherited retinal degeneration: PARP-Dependent activation of calpain requires CNG Channel activity. Biomolecules. 2022;12(3):455.
17. Barabas P, Peck CC, Krizaj D. Do calcium channel blockers rescue dying photoreceptors in the Pde6b rd1 mouse? In: Retinal degenerative diseases. 2010. p. 491–9.
18. Takano Y, et al. Study of drug effects of calcium channel blockers on retinal degeneration of rd mouse. Biochem Biophys Res Commun. 2004;313(4):1015–22.
19. Paquet-Durand F, et al. A key role for cyclic nucleotide gated (CNG) channels in cGMP-related retinitis pigmentosa. Hum Mol Genet. 2011;20(5):941–7.
20. Das S, et al. Redefining the role of Ca2+-permeable channels in photoreceptor degeneration using diltiazem. Cell Death Dis. 2022;13(1):1–13.
21. Pearce-Kelling SE, et al. Calcium channel blocker D-cis-diltiazem does not slow retinal degeneration in the PDE6B mutant rcd1 canine model of retinitis pigmentosa. Mol Vis. 2001;7:42.
22. Dolphin AC. Voltage-gated calcium channels and their auxiliary subunits: physiology and pathophysiology and pharmacology. J Physiol. 2016;594(19):5369–90.

23. Catterall WA, Goldin AL, Waxman SG. International Union of Pharmacology. XLVII. Nomenclature and structure-function relationships of voltage-gated sodium channels. Pharmacol Rev. 2005;57(4):397–409.
24. Tykocki NR, Jackson WF, Watts SW. Reverse-mode Na+/Ca2 + exchange is an important mediator of venous contraction. Pharmacol Res. 2012;66(6):544–54.
25. Yu SP, Choi DW. Na+—Ca2 + exchange currents in cortical neurons: concomitant forward and reverse operation and effect of glutamate. Eur J Neurosci. 1997;9(6):1273–81.
26. Khananshvili D. The SLC8 gene family of sodium–calcium exchangers (NCX)–Structure, function, and regulation in health and Disease. Mol Aspects Med. 2013;34(2–3):220–35.
27. Emrich SM, Yoast RE, Trebak M. Physiological functions of CRAC channels. Annu Rev Physiol. 2022;84:355–79.
28. Tang PH, et al. Phenotypic variance in Calpain-5 retinal degeneration. Am J Ophthalmol case Rep. 2020;18:100627.
29. Baudry M, et al. Role of Calpain-1 in neurogenesis. Front Mol Biosci. 2021;8:685938.
30. Wang Y, et al. Calpain-1 and Calpain-2 in the brain: new evidence for a critical role of Calpain-2 in neuronal death. Cells. 2020;9(12):2698.
31. Baudry M, Bi X. Calpain-1 and calpain-2: the Yin and Yang of synaptic plasticity and neurodegeneration. Trends Neurosci. 2016;39(4):235–45.
32. Briz V, Baudry M. Calpains: master regulators of synaptic plasticity. Neuroscientist. 2017;23(3):221–31.
33. Perrin BJ, Amann KJ, Huttenlocher A. Proteolysis of cortactin by calpain regulates membrane protrusion during cell migration. Mol Biol Cell. 2006;17(1):239–50.
34. Baudry M. Calpain-1 and calpain-2 in the brain: Dr. Jekill and Mr Hyde? Curr Neuropharmacol. 2019;17(9):823–9.
35. Sanyal S, Bal AK. Comparative light and electron microscopic study of retinal histogenesis in normal and rd mutant mice. Z für Anatomie und Entwicklungsgeschichte. 1973;142(2):219–38.
36. Sancho-Pelluz J, et al. Photoreceptor cell death mechanisms in inherited retinal degeneration. Mol. Neurobiol. 2008;38:253–69.
37. Aït-Ali N, et al. Rod-derived cone viability factor promotes cone survival by stimulating aerobic glycolysis. Cell. 2015;161(4):817–32.
38. Chen Y, et al. Single-cell transcriptomic profiling in inherited retinal degeneration reveals distinct metabolic pathways in rod and cone photoreceptors. Int J Mol Sci. 2022;23(20):12170.
39. Thomas JG, et al. An efficient and robust statistical modeling approach to discover differentially expressed genes using genomic expression profiles. Genome Res. 2001;11(7):1227–36.
40. Zaim SR, et al. Personalized beyond precision: designing unbiased gold standards to improve single-subject studies of personal genome dynamics from gene products. J Personalized Med. 2020;11(1):24.
41. Caffé AR, et al. A combination of CNTF and BDNF rescues rd photoreceptors but changes rod differentiation in the presence of RPE in retinal explants. IOVS. 2001;42(1):275–82.
42. Belhadj Z, et al. A combined "eat me/don't eat me" strategy based on extracellular vesicles for anticancer nanomedicine. J Extracell Vesicles. 2020;9(1):1806444.
43. Belhadj S, et al. Long-term, serum-free cultivation of organotypic mouse retina explants with intact retinal pigment epithelium. J Vis Exp. 2020;165:e61868.
44. Wie MB, et al. BAPTA/AM, an intracellular calcium chelator, induces delayed necrosis by lipoxygenase-mediated free radicals in mouse cortical cultures. Prog Neuropsychopharmacol Biol Psychiatry. 2001;25(8):1641–59.
45. Das S, et al. Redefining the role of Ca2+-permeable channels in photoreceptor degeneration using diltiazem. Cell Death Dis. 2022;13(1):47.
46. Waldron RT, et al. The Orai Ca2 + channel inhibitor CM4620 targets both parenchymal and immune cells to reduce inflammation in experimental acute pancreatitis. J Physiol. 2019;597(12):3085–105.
47. NIU, C.F., et al. Electrophysiological effects of SN-6, a novel Na+/Ca2 + exchange inhibitor on membrane currents in guinea pig ventricular myocytes. Ann N Y Acad Sci. 2007;1099(1):534–9.
48. Kraus RL, et al. In vitro characterization of T-type calcium channel antagonist TTA-A2 and in vivo effects on arousal in mice. J Pharmacol Exp Ther. 2010;335(2):409–17.
49. Domon Y, et al. Binding characteristics and analgesic effects of mirogabalin, a novel ligand for the α2δ subunit of voltage-gated calcium channels. J Pharmacol Exp Ther. 2018;365(3):573–82.
50. Wang Y, et al. A molecular brake controls the magnitude of long-term potentiation. Nat Commun. 2014;5(1):3051.
51. Belhadj S, et al. Fluorescent detection of PARP activity in unfixed tissue. PLoS One. 2021;16(1):e0245369.
52. Larbig R, et al. Activation of reverse Na+–Ca2 + exchange by the na + current augments the cardiac Ca2 + transient: evidence from NCX knockout mice. J Physiol. 2010;588(17):3267–76.
53. Li S, et al. CaMKII potentiates store-operated Ca2 + entry through enhancing STIM1 aggregation and interaction with Orai1. Cell Physiol Biochem. 2018;46(3):1042–54.
54. Belhadj S, et al. Long-term, serum-free cultivation of organotypic mouse retina explants with intact retinal pigment epithelium. J Vis Exp. 2020;(165):e61868.
55. Paquet-Durand F, et al. Calpain is activated in degenerating photoreceptors in the rd1 mouse. J Neurochem. 2006;96(3):802–14.
56. Power MJ, et al. Systematic spatiotemporal mapping reveals divergent cell death pathways in three mouse models of hereditary retinal degeneration. J Comp Neurol. 2020;528(7):1113–39.
57. Wang Y, et al. A molecular brake controls the magnitude of long-term potentiation. Nat Commun. 2014;5(1):1–12.
58. Sedgwick P. Spearman's rank correlation coefficient. BMJ. 2014;349:g7327.
59. Fang EF, et al. Defective mitophagy in XPA via PARP-1 hyperactivation and NAD+/SIRT1 reduction. Cell. 2014;157(4):882–96.
60. Fox DA, Poblenz AT, He L. Calcium overload triggers rod photoreceptor apoptotic cell death in chemical-induced and inherited retinal degenerations. Ann N Y Acad Sci. 1999;893(1):282–5.
61. Vallazza-Deschamps G, et al. Excessive activation of cyclic nucleotide-gated channels contributes to neuronal degeneration of photoreceptors. Eur J Neurosci. 2005;22(5):1013–22.
62. Das S, et al. The role of cGMP-signalling and calcium-signalling in photoreceptor cell death: perspectives for therapy development. Pflügers Arch. 2021;473(9):1411–21.
63. Barabas P, Peck CC, Krizaj D. Do calcium channel blockers rescue dying photoreceptors in the Pde6b rd1 mouse? In: Retinal degenerative diseases: laboratory and therapeutic investigations. 2010. p. 491–9.
64. Clapham DE. Calcium signaling. Cell. 2007;131(6):1047–58.
65. Comitato A, et al. Pigment epithelium-derived factor hinders photoreceptor cell death by reducing intracellular calcium in the degenerating retina. Cell Death Dis. 2018;9(5):1–13.
66. Feng H, et al. Deficiency of calcium and magnesium induces apoptosis via scavenger receptor BI. Life Sci. 2011;88(13–14):606–12.
67. Vinberg F, Chen J, Kefalov VJ. Regulation of calcium homeostasis in the outer segments of rod and cone photoreceptors. Prog Retin Eye Res. 2018;67:87–101.
68. Michalakis S, Becirovic E, Biel M. Retinal cyclic nucleotide-gated channels: from pathophysiology to therapy. Int J Mol Sci. 2018;19(3):749.
69. Koch S, et al. Gene therapy restores vision and delays degeneration in the CNGB1–/– mouse model of retinitis pigmentosa. Hum Mol Genet. 2012;21(20):4486–96.
70. Tanwar J, Motiani RK. Role of SOCE architects STIM and Orai proteins in cell death. Cell Calcium. 2018;69:19–27.
71. Karademir D, et al. Single-cell RNA sequencing of the retina in a model of retinitis pigmentosa reveals early responses to degeneration in rods and cones. BMC Biol. 2022;20(1):1–19.
72. Inokuchi Y, et al. A Na+/Ca2 + exchanger isoform, NCX1, is involved in retinal cell death after N-methyl-d-aspartate injection and ischemia–reperfusion. J Neurosci Res. 2009;87(4):906–17.
73. Iwamoto T, et al. The exchanger inhibitory peptide region-dependent inhibition of Na+/Ca2 + exchange by SN-6 [2-[4-(4-nitrobenzyloxy) benzyl] thiazolidine-4-carboxylic acid ethyl ester], a novel benzyloxyphenyl derivative. Mol Pharmacol. 2004;66(1):45–55.
74. Paquet-Durand F, et al. PKG activity causes photoreceptor cell death in two retinitis pigmentosa models. J Neurochem. 2009;108(3):796–810.
75. Power M, et al. Cellular mechanisms of hereditary photoreceptor degeneration–Focus on cGMP. Prog Retin Eye Res. 2020;74:100772.

76. Catterall WA. Voltage-gated calcium channels. Cold Spring Harb Perspect Biol. 2011;3(8):a003947.
77. Campiglio M, Flucher BE. Flucher, the role of auxiliary subunits for the functional diversity of voltage-gated calcium channels. J Cell Physiol. 2015;230(9):2019–31.
78. Tang L, et al. Structural basis for diltiazem block of a voltage-gated Ca2 + channel. Mol Pharmacol. 2019;96(4):485–92.
79. Domon Y, et al. Binding characteristics and analgesic effects of mirogabalin, a novel ligand for the α2δ subunit of voltage-gated calcium channels. J Pharmacol Exp Ther. 2018;365(3):573–82.
80. Kraus RL, et al. In vitro characterization of T-type calcium channel antagonist TTA-A2 and in vivo effects on arousal in mice. J Pharmacol Exp Ther. 2010;335(2):409–17.
81. Pawlyk BS, et al. Absence of photoreceptor rescue with D-cis-diltiazem in the rd mouse. IOVS. 2002;43(6):1912–5.
82. Schön C, Paquet-Durand F, Michalakis S. Cav1. 4 L-type calcium channels contribute to calpain activation in degenerating photoreceptors of rd1 mice. PLoS One. 2016;11(6):e0156974.
83. Kopecky BJ, Liang R, Bao J. T-type calcium channel blockers as neuroprotective agents. PloS One. 2014;466(4):757–65.
84. Kawai F, et al. Na + action potentials in human photoreceptors. Neuron. 2001;30(2):451–8.
85. Yan J, et al. Inherited retinal degeneration: PARP-Dependent activation of calpain requires CNG channel activity. Biomolecules. 2022;12(3):455.
86. Nian H, Ma B. Calpain–calpastatin syst cancer progression. Biol Rev. 2021;96(3):961–75.
87. Luo Y, Sellitti DF, Suzuki K. The calpain proteolytic system. In: Encyclopedia of cell biology. 2016.
88. Shinkai-Ouchi F, et al. Calpain-2 participates in the process of calpain-1 inactivation. Biosci Rep. 2020;40(11):BSR20200552.
89. Paquet-Durand F, et al. Photoreceptor rescue and toxicity induced by different calpain inhibitors. J Neurochem. 2010;115(4):930–40.
90. Schaefer KA, et al. Calpain-5 expression in the retina localizes to photoreceptor synapses. IOVS. 2016;57(6):2509–21.
91. Wert KJ, et al. CAPN5 mutation in hereditary uveitis: the R243L mutation increases calpain catalytic activity and triggers intraocular inflammation in a mouse model. Hum Mol Genet. 2015;24(16):4584–98.
92. Vu JT, et al. Calpains as mechanistic drivers and therapeutic targets for ocular Disease. Trends in molecular medicine; 2022.
93. Wert KJ, et al. CAPN5 mutation in hereditary uveitis: the R243L mutation increases calpain catalytic activity and triggers intraocular inflammation in a mouse model. Hum Mol Genet. 2015;24(16):4584–98.
94. Paquet-Durand F, et al. Excessive activation of poly (ADP-ribose) polymerase contributes to inherited photoreceptor degeneration in the retinal degeneration 1 mouse. J Neurosci. 2007;27(38):10311–9.
95. Sancho-Pelluz J, et al. Excessive HDAC activation is critical for neurodegeneration in the rd1 mouse. Cell Death Dis. 2010;1(2):e24–e24.
96. Ray Chaudhuri A, Nussenzweig A. The multifaceted roles of PARP1 in DNA repair and chromatin remodelling. Nat Rev Mol Cell Biol. 2017;18(10):610–21.
97. David KK, et al. Parthanatos a messenger of death. Front Biosci (Schol Ed). 2009;14:1116.
98. Sahaboglu A, et al. Drug repurposing studies of PARP inhibitors as a new therapy for inherited retinal degeneration. Cell Mol Life Sci. 2020;77(11):2199–216.
99. Geistrikh I, et al. Ca2+-induced PARP-1 activation and ANF expression are coupled events in cardiomyocytes. Biochem J. 2011;438(2):337–47.
100. Zhang F, et al. PARP-1 hyperactivation and reciprocal elevations in intracellular Ca2 + during ROS-induced nonapoptotic cell death. Toxicol Sci. 2014;140(1):118–34.
101. Görlach A, et al. Calcium and ROS: a mutual interplay. Redox Biol. 2015;6:260–71.
102. Srinivas US, et al. ROS and the DNA Damage Response in cancer. Redox Biol. 2019;25:101084.
103. Milazzo G, et al. Histone deacetylases (HDACs): evolution, specificity, role in transcriptional complexes, and pharmacological actionability. Genes. 2020;11(5):556.
104. Cohen MS. And development, interplay between compartmentalized NAD + synthesis and consumption: a focus on the PARP family. Genes Dev. 2020;34(5–6):254–62.
105. Chung HT, Joe Y. Antagonistic crosstalk between SIRT1, PARP-1, and-2 in the regulation of chronic inflammation associated with aging and metabolic diseases. Integr Med Res. 2014;3(4):198–203.
106. Romeo-Guitart D et al. SIRT1 activation with neuroheal is neuroprotective but SIRT2 inhibition with AK7 is detrimental for disconnected motoneurons. Cell Death Dis. 2018;9(5):1–14.
107. Seo J, et al. Trichostatin A epigenetically increases calpastatin expression and inhibits calpain activity and calcium-induced SH-SY 5 Y neuronal cell toxicity. FEBS J. 2013;280(24):6691–701.
108. Liu W, et al. Metabolic stress-induced cardiomyopathy is caused by mitochondrial dysfunction due to attenuated Erk5 signaling. Nat. Commun. 2017;8(1):1–16.
109. Zhang Y, Xu H. Translational regul mitochondrial biogenesis. Biochem Soc Trans. 2016;44(6):1717–24.
110. Chen L, et al. PGC-1α-mediated mitochondrial quality control: molecular mechanisms and implications for heart failure. 2022. p. 1076.

Publisher's Note